View metadata, citation and similar papers at core.ac.uk

brought to you by CORE

provided by University of Bergen

Received: 27 September 2018 | Revised: 18 December 2019 | Accepted: 19 December 2019

DOI: 10.1096/fj.201802061RR

RESEARCH ARTICLE

THE FASEB JOURNAL

Tyrosine kinase inhibitors and interferon-α increase tunneling nanotube (TNT) formation and cell adhesion in chronic myeloid leukemia (CML) cell lines

Maria Omsland[1,2] | Vibeke Andresen[1,3] | Stein-Erik Gullaksen[1,3] | Pilar Ayuda-Durán[4] | Mihaela Popa[3,5] | Randi Hovland[6] | Atle Brendehaug[6] | Jorrit Enserink[4] | Emmet McCormack[1] | Bjørn Tore Gjertsen[1,3]

[1]Centre for Cancer Biomarkers CCBIO, Department of Clinical Science, University of Bergen, Bergen, Norway

[2]Animal Models and Retroviral Vaccines Section, Vaccine Branch, National Cancer Institute, National Institutes of Health, Bethesda, MD, USA

[3]Department of Internal Medicine, Hematology Section, Haukeland University Hospital, Bergen, Norway

[4]Department of Molecular Cell Biology, Institute for Cancer Research, The Norwegian Radium Hospital, Oslo University Hospital, Oslo, Norway

[5]KinN Therapeutics, Bergen, Norway

[6]Department of Medical Genetics, Haukeland University Hospital, Bergen, Norway

Correspondence
Bjørn Tore Gjertsen, Centre for Cancer Biomarkers CCBIO, Department of Clinical Science, University of Bergen, Bergen N-5021, Norway.
Email: bjorn.gjertsen@uib.no

Funding information
University of Bergen; Intramural Research Program of the National Institutes of Health; National Cancer Institute; Center for Cancer Research; Norwegian Cancer Society with Solveig & Ole Lunds Legacy and Øyvinn Mølbach-Petersens Fond for Clinical Research (BTG); Melzer Høyskolefond (BTG); Bergen Forskningsstiftelse (Bergen Research Foundation); Trond Mohn Foundation (VA); Helse Vest RHF; Helse Bergen HF, Grant/Award Number: 911809, 911852, 912171 and 240222; Norwegian Cancer Society, Grant/Award Number: 205729 and 182524; Norwegian Research Council of Norway through its Centers of excellence funding scheme, Grant/Award Number: 223250 and 262652; Norwegian Research Council, Grant/Award Number: 294916

Abstract

Chronic myeloid leukemia (CML) is a stem cell disease of the bone marrow where mechanisms of inter-leukemic communication and cell-to-cell interactions are proposed to be important for optimal therapy response. Tunneling nanotubes (TNTs) are novel intercellular communication structures transporting different cargos with potential implications in therapy resistance. Here, we have investigated TNTs in CML cells and following treatment with the highly effective CML therapeutics tyrosine kinase inhibitors (TKIs) and interferon-α (IFNα). CML cells from chronic phase CML patients as well as the blast crisis phase cell lines, Kcl-22 and K562, formed few or no TNTs. Treatment with imatinib increased TNT formation in both Kcl-22 and K562 cells, while nilotinib or IFNα increased TNTs in Kcl-22 cells only where the TNT increase was associated with adherence to fibronectin-coated surfaces, altered morphology, and reduced movement involving β1integrin. *Ex vivo* treated cells from chronic phase CML patients showed limited changes in TNT formation similarly to bone marrow cells from healthy individuals. Interestingly, in vivo nilotinib treatment in a Kcl-22 subcutaneous mouse model resulted in morphological changes and TNT-like structures in the tumor-derived Kcl-22 cells. Our results demonstrate that CML cells express low levels of TNTs, but CML therapeutics increase TNT formation in designated cell models indicating TNT functionality in bone marrow derived malignancies and their microenvironment.

Abbreviations: CML, chronic myeloid leukemia; IFNα, interferon-α; TNT, tunneling nanotube; TKI, tyrosine kinase inhibitor.

This is an open access article under the terms of the Creative Commons Attribution-NonCommercial License, which permits use, distribution and reproduction in any medium, provided the original work is properly cited and is not used for commercial purposes.
© 2020 The Authors. The FASEB Journal published by Wiley Periodicals, Inc. on behalf of Federation of American Societies for Experimental Biology

KEYWORDS
cell adhesion, chronic myeloid leukemia, interferon-α, tunneling nanotubes, tyrosine kinase inhibitors

1 | INTRODUCTION

Chronic myeloid leukemia (CML) is a myeloid stem cell disease characterized by the tyrosine kinase BCR-ABL1 fusion protein derived from the chromosomal translocation *t* (9;22), involving bone marrow and spleen in the chronic phase. Initially, CML treatment included interferon-α (IFNα) and hematopoietic stem cell transplantation.[1,2] The introduction of IFNα revolutionized the treatment of CML and initial studies performed in 1980s by Talpaz and colleagues resulted in the first evidence of induced hematological remission and cytogenetic responses in a subset of treated patients.[3,4] This was the first-line treatment of choice for CML prior to the introduction of the tyrosine kinase inhibitor (TKI) imatinib in 2000, but IFNα is now gaining enhanced interest in combination treatments with imatinib and other TKIs.[5] Imatinib was the first of a series of BCR-ABL1-targeted drugs used in treatment of CML patients, and these inhibitors vary based on potency, efficiency on mutated ABL1 and have different adverse effect profiles.[6-8] The role of BCR-ABL1 in microenvironment dependent cellular communication is less understood[9-11] particularly in the context of the efficient therapies with small molecule kinase inhibitors.[12-14]

It is well established that the tumor microenvironment and its cell-to-cell interactions play a pivotal role in the outcome of cancer therapy.[15] One modality of physical cell-to-cell interaction is the tunneling nanotube (TNT).[16] TNTs are defined as thin (50-200 nm), fragile, and dynamic structures, consisting of plasma membrane and filamentous (F)-actin.[16,17] They are involved in cell-to-cell interaction and intercellular transport of organelles and pathogens such as virus and bacteria.[16,18-24] Leukocytes, their leukemic counterparts and bone marrow stromal cells have all been reported to form TNTs in vitro.[25-32] TNT is proposed to be a mechanism for chemo resistance by transport of oncoproteins between T and B cells as well as in colon cancer cells, by transfer of mitochondria from endothelial cells to chemotherapy exposed cancer cells, or by induced drug-efflux in aggressive forms of pancreatic carcinoma.[33-38] The impact of TNTs in vivo is so far not well characterized, but they have been described to connect myeloid cells in the cornea of mouse[39,40] and in fresh resected tumor samples from patients with malignant pleural mesothelioma and lung adenocarcinoma.[41] Subsequently, TNTs have been proposed to be implicated in disease and to play a role with respect to therapy response recently demonstrated by vesicle exchange from stromal cells to CML cells providing increased resistance to imatinib.[42,43]

The BCR-ABL1 protein contains an F-actin binding domain and orchestrates several cellular processes including actin processing, cell attachment to fibronectin and cell migration.[44] Features of CML progenitor cells from patients in the chronic phase include decreased adhesion and low affinity to fibronectin coated surfaces compared to normal counterparts.[45] IFNα treatment has been demonstrated to increase adhesion of CML progenitor cells to bone marrow stromal cells.[46-48] Restoration of the adhesion defect in CML cells seems therefore to be a significant feature of the effective CML therapy, recently revisited in the therapeutic combination of TKIs and IFNα eradicating CML progenitor cells resulting in non-detectable disease.[5,49] Here, we investigate the role of TKIs and IFNα treatment on TNT formation in CML cell models connecting TNT formation to increased cell attachment to fibronectin coated surfaces.

2 | MATERIALS AND METHODS

2.1 | Cell lines

K562, Kcl-22 (ATCC and DSMZ), and Ba/F3 cells (kind gift to Prof. Enserink from Dr. Gordon B. Mills laboratory, Portland, Oregon, USA), were routinely tested for mycoplasma and cultured according to provider's instructions. RPMI-1640 medium was supplemented with 10% of FBS, 1% of L-glutamine (2 mM), and 1% of (1.0 U/mL) penicillin and streptomycin (5 mM) (Sigma-Aldrich). The RPMI-1640 medium for the IL-3 dependent Ba/F3 cells were additionally supplemented with 10% conditioned medium from WEHI3B cells (mouse myelomonocytic cell line) known to secrete high concentrations of IL-3.[50] The WEHI3B cells were grown to confluency in a T75 flask with complete IMDM medium (containing 10% of FBS, 1% of Pen-Strep and L-glutamine), and cultured for 2-3 days before the supernatant was centrifuged at 1500 RPM for 10 minutes and sterile filtered through a 0.2 μm filter.

2.2 | MemGFP, memCherry, and mitoGFP transduced cells

The Kcl-22(memGFP), K562(memGFP), and Kcl-22(memCherry) cells were generated by transducing the cells with ready-to-use lentiviral particles expressing a membrane (mem) localization signal (20 amino acids of the N-terminal part of neuromodulin, containing a palmitoylation signal)

fused to GFP or Cherry; rLV-EF1-AcGFP-Mem-9 (Takara, rV2.1A1.1942 C2/rV2.1A1.2001 C2) and the Kcl-22(mito-GFP) cells were generated by transducing the cells with ready-to-use lentiviral particles expressing a mitochondria targeting sequence (mito) fused to GFP; rLV.EF1.AcGFP-Mito-9 (Takara, rV2.1A1.1941 C2) according to the provider's instructions. The transduced cells were sorted using BD FACS Aria SORP at the Flow Cytometry Core Facility, Department of Clinical Science, University of Bergen, Norway.

2.3 | Primary bone marrow cells

The study was conducted in accordance with the Declaration of Helsinki and approved by the local Ethics Committee (Regional Ethics Committee West projects 2012/2245 and 2012/2247, University of Bergen, Norway). Bone marrow samples from ten consecutively diagnosed CML patients and three healthy donors were collected after informed consent and were processed by density gradient separation (Lymphoprep, Axis-Shield, Oslo, Norway).[51] For the bone marrow patient samples and healthy donors (Samples 5-14, Supplementary Table 1), hematopoietic progenitor cells were sorted by EasySep magnetic negative selection (StemCell Technologies, #19056). Briefly, both unsorted and positive and negative sorted cells were investigated for the presence of TNTs before and after treatment with nilotinib, imatinib, or IFNα, dependent on number of cells available after sorting. Total bone marrow samples (Samples 5-10 and 13, Supplementary Table 1) and two positive sorted bone marrow samples (Samples 7 and 10, Supplementary Table 1) were fixed and analyzed (and reanalyzed) for the presence of BCR-ABL1 by fluorescent interphase in situ hybridization (FISH). Interphase FISH analysis was performed using the BCR/ABL1 dual color fusion probe from Vysis Abbott according to manufactures instructions. Signal pattern were scored in 70 to 320 informative cells per sample.

2.4 | Doxycycline inducible Ba/F3 cells

BCR-ABL1 (P210) was cloned into pcDNA3 (Addgene) after EcoRI digestion. The orientation and sequence was verified by PCR. This was further sub-cloned into the EcoRI site of PLVX-tetOne-Puro (from the Lenti-X Tet-One Inducible Expression Systems). Ba/F3 cells were transfected with 2 μg of the PLVX-tetOne-BCR-ABL1 plasmid or PLVX-tetOne-empty vector by electroporation (Amaxa biosystems nucleofector II: program U20) using Ingenio Electroporation solution (catalog number MIR 50114). Transfected cells were cultured in medium for 24-72 hours before selection with 1 μg/ml puromycin. Puromycin resistant clones were sorted and grown independently; cells were continually cultured in medium with puromycin to maintain selection pressure. Doxycycline (0.1 μg/mL) was added to induce expression of BCR-ABL1.

2.5 | Antibodies and reagents

The following primary antibodies were used for immunofluorescence and/or immunoblotting: anti-β-tubulin (clone TUB 2.1, Sigma-Aldrich, 1:1000), anti-COX IV (ab16056, 1:2500), anti-cAbl ((24-11) sc-23, Santa Cruz Biotechnology, 1:1000), anti-integrin β1 blocking antibody [P5D2] (ab24693, Abcam). Secondary antibodies used for immunofluorescence or immunoblotting; Alexa Fluor 488- or 594-conjugated goat-anti-mouse (Invitrogen, 1:5000), horseradish peroxidase (HRP)-conjugated goat anti-rabbit/mouse (Jackson Immunoresearch, 1:10 000). The following were used for actin and membrane staining: Alexa Fluor 350-conjugated phalloidin and wheat germ agglutinin (WGA)–Alexa Fluor 594 or 488 (Invitrogen) as previously described.[31] TKIs: imatinib, nilotinib, bosutinib, ponatinib, and dasatinib (Selleckchem). IFNα (Intron A from MSD), Cytochalasin D (Sigma-Aldrich), doxycycline (Doxyferm, Nordic Drugs AB, Limhamn), puromycin (Sigma-Aldrich), Bovine serum albumin (BSA) fraction V (Roche), fibronectin (Sigma-Aldrich). Optimal antibody concentrations were determined for all antibodies used.

2.6 | TNT identification and quantification

A TNT in this study is defined as a thin straight structure, ≤ 200 nm in diameter, minimum 5 μm in length, hovering above the substratum, connecting two cells. TNTs were distinguished from cytoplasmic bridges, which appear following cell division, by the lack of a midbody clearly visible by differential interference contrast and/or staining of cellular membranes.[31] 8-well μ-slides (Ibidi GmbH) were pre-coated with fibronectin (10 μg/mL, F2006, Sigma-Aldrich) for 30 minutes at 37°C before washed with saline. 70 000 cells were seeded per well and incubated overnight under physiological conditions. Primary CML cells were seeded in IMDM medium containing 20% of FBS overnight and stained with wheat germ agglutinin conjugated with Alexa Fluor 488 or 594 (1.67 μg/mL) as previously described.[31] Cells were examined live by fluorescent light microscopy (Zeiss Axio Observer Z1 with AxioVision 4.8.2 or Zen software) using a 63X/1.4 NA Oil DICIII objective, heat block (37°C) and standard air conditions. 100 cells per well were counted following a fixed counting pattern with 5-6 cells examined per vision field. The result is described as number of TNTs/100 cells meaning the total number of TNTs (one TNT always connects two cells) among 100 cells counted. For further details, see Supplementary Figure in Omsland et al.[31] Cell

viability was monitored by Hoechst 33342 nucleic acid stain (Sigma) as previously described (Zeiss Axio Observer A1with LD Plan Neofluar 20X/0.4 Corr Ph2).[52]

2.7 | Scanning electron microscopy (SEM)

K562 (50 000) cells were seeded onto L-lysine pre-coated coverslips followed by incubation at 37°C overnight before fixed (4% of glutaraldehyde in 0.2 M Na-cacodylate in buffer diluted 1:1 with medium) for 2 hours at RT. Cells were washed carefully three times for 15 minutes with 0.1 M Na-cacodylate buffer followed by a 60 minutes post-fixation with 1% of osmiumtetraoxide in 0.1 M Na-cacodylate buffer and washed twice for 10 minutes with 0.1 M Na-cacodylate buffer. Dehydration with ethanol was performed with 30% for 15 minutes, 50% for 15 minutes, 70% for 20 minutes, or overnight, 96% for 20 minutes and twice with 100% for 20 minutes. The coverslips were obtained from the wells and placed on SEM stubs before incubated in a heat-incubator overnight. Critical point drying was omitted in order to avoid breakage of TNTs. The SEM stubs were coated with 5-10 nm gold/palladium before SEM microscopy.

2.8 | Mass cytometry

To reduce experiment variability and antibody consumption, the commercially available metal barcoding kit from Fluidigm was used. After cell barcoding and washing according to the manufacturers' recommendations, uniquely barcoded samples were pooled for further processing for mass cytometry analysis.

The pooled cell sample was stained with a panel of cell surface markers (30 minutes, RT), washed using Cell Staining Buffer (CSB) (Fluidigm) and permeabilized with methanol (−20°C). After washing with CSB, the cell sample was stained with intracellular phospho-specific antibodies (30 minutes, RT). The sample was washed with CSB and re-suspended in the buffer containing iridium-intercalator (natural isotopic abundance of iridium $Ir^{191/193}$), which intercalates iridium into the DNA (1 hours, 4°C). The sample was washed with CSB and pelleted by centrifugation following incubation. Immediately prior to data acquisition cells were re-suspended to a final concentration of approximately 5×10^5 cells/mL in MaxPar water (Fluidigm) containing normalization beads (Fluidigm) diluted 1:10 and analyzed on a Helios mass cytometer (Fluidigm), placed in the Flow Cytometry Core Facility of Bergen, University of Bergen. Any drift in the data resulting from loss of detector sensitivity was corrected for using the normalization bead data. An automatic barcode deconvolution algorithm developed by Zunder et al[53] was used to identify each uniquely barcoded sample. Further discrimination and gating of single cells was achieved by plotting all events by DNA-content (Ir^{191} or Ir^{103}) versus Event Length (number of pushes). Together, barcode deconvolution and gating of cells on DNA content versus event length, is an effective filter for removal of doublets and identification of single cells. Finally, cleaved caspase-3 readily discriminated between apoptotic and non-apoptotic cells, where non-apoptotic cells were used for statistical analysis. A detailed overview of the antibody panel is described in Table 1.

2.9 | Blocking of β1 integrin

Cells were cultured in 6-well plates with a density of 0.7×10^6 cells/mL. Cells were incubated in medium with or without 10 μg/mL of anti-β1 integrin [P5D2] antibody for 30 minutes before seeded on fibronectin pre-coated μ-slides (Ibidi GmbH). Cells were incubated for 3 hours to allow attachment before treatment with 1 μM nilotinib or 100 U/mL IFNα for 1 hours prior to examination by live microscopy.

2.10 | Cell tracking

Measuring of cell area was performed manually using ImageJ: Images were analyzed as 8-bit files using FFT Bandpass Filter, threshold was set manually and adjusted until cells were distinguished from the background>convert to mask>fill holes>cells in close proximity were then distinguished using watershed algorithm. Measuring of the cell area was performed using the measure tool under the region of interest manager tool and single cells were selected using the wand tool.

Tracking of cells was performed using metamorph and the chemotaxis and migration (Ibidi GmbH) plugin to ImageJ was performed to calculate accumulated distance and to make trajectory plots as described by Hurley et al.[54]

2.11 | Immunofluorescence

The presence of F-actin and/or microtubules in TNTs was investigated in Kcl-22 cells (on 8-well μ-slides, Ibidi GmbH) fixed in 4% of PFA in PBS and 0.2% of glutaraldehyde in PBS for 20 minutes at room temperature (RT) followed by one wash with PBS, before permeabilized for 1 minute using 0.2% of Tween in PBS and washed twice with PBS. Cells were blocked with 0.5% of BSA PBS for 20 minutes at RT and then incubated for 1 hour at RT in the dark with 33 nM Alexa Fluor phalloidin, washed once with PBS and incubated with anti-β-tubulin antibody (1:200 in blocking solution) overnight at 4°C. Then cells were washed twice with

TABLE 1 Antibody panel for mass cytometry

A.m.u	Metal	Epitope	Clone	Vendor
102	Pd	Metal Barcode Channel #1	N.A.	Fluidigm
104	Pd	Metal Barcode Channel #2	N.A.	Fluidigm
105	Pd	Metal Barcode Channel #3	N.A.	Fluidigm
106	Pd	Metal Barcode Channel #4	N.A.	Fluidigm
108	Pd	Metal Barcode Channel #5	N.A.	Fluidigm
110	Pd	Metal Barcode Channel #6	N.A.	Fluidigm
89	Y	CD45	HI30	Fluidigm
141	Pr	pBCR Y177	Polyclonal	CST
142	Nd	Caspase 3 Cleaved	D3E9	Fluidigm
143	Nd	pCrkL [Y207]	Polyclonal	Fluidigm
149	Sm	p4E-BP1	236B4	Fluidigm
150	Nd	pStat5 [Y694]	47	Fluidigm
153	Eu	pStat1 [Y701]	58D6	Fluidigm
154	Sm	pAbl Y245	73E5	CST
156	Gd	p-p38 [T180/Y182]	D3F9	Fluidigm
158	Gd	pStat3 [Y705]	4/P-STAT3	Fluidigm
165	Ho	pCREB [S133]	4/P-STAT3	Fluidigm
167	Yb	pERK 1/2 [T202/Y204]	D1314.4E	Fluidigm
172	Yb	pS6 [S235/S236]	N7-548	Fluidigm
176	Yb	pS6 [S240/S244]	D68F8	CST
191	Ir	DNA	N.A.	Fluidigm
193ß	Ir	DNA	N.A.	Fluidigm

Abbreviations: A.M.U, atomic mass unit; CST, cell signaling technology; Metal, rare metal isotopes.

PBS and incubated with Alexa Fluor-488 or Alexa Fluor-594 goat-anti-mouse antibodies (1:5000 in blocking solution) for 1 hour at RT, before washed twice with PBS and examined by fluorescence microscopy. Cells not expressing memGFP were stained with wheat germ agglutinin (WGA) conjugated with Alexa Fluor-488 or Alexa Fluor-594 for 8 minutes followed by one wash with PBS before examined by microscopy and manual quantification of TNTs.

2.12 | Immunoblotting

Cells were lysed and analyzed by immunoblotting according to standard protocol.[55,56] Briefly, immunobloting was performed using precast gels from BioRad, transferred to PVDF membranes using Pierce G2 fast blotter (Thermo Scientific). Membranes were blocked for 1 hours at RT in 5% of fat-free dry-milk or 5% of BSA in TBST, incubated with primary antibody at 4°C overnight. Membranes were washed with TBST followed by incubation for 1 hour with secondary antibody ([HRP]-conjugated goat-anti-rabbit/mouse) was diluted 1:1000 in 5% of drymilk in TBST and washed with TBST before developed using SuperSignal West pico or femto (Thermo Fisher Scientific). Developed immunoblots were detected and captured by ImageQuant LAS 4000 (GE Healthcare Life Sciences).

2.13 | Transfer assay

Kcl-22(memCherry) cells (35 000) and Kcl-22(mitoGFP) cells (35 000) were seeded on a fibronectin pre-coated 8-well μ-slides (IBIDI) and treated with 100 U/mL IFNα for 24 hours before fixation with 4% of PFA for 15 minutes at room temperature in the dark. The experiment was performed in duplicates and in total six images was obtained from each well and presence of memCherry or mitoGFP was counted.

2.14 | Animal studies

2.14.1 | NSG (NOD/SCID IL2rγ^{null}) mice

The protocol for animal studies was approved by the Norwegian State Commission for Laboratory Animals (FOTS approval number: 20158178) and the experiments were performed according to the European Convention for the Protection of Vertebrates Used for Scientific Purposes.

NSG mice (6-8 weeks old; Vivarium, University of Bergen) were maintained under defined flora conditions in individually ventilated cage on a 12 hours dark/night schedule at a constant temperature of 21°C and at 50% relative humidity. Bedding and cages were autoclaved and changed twice per month. The mice had continuous supply of sterile water and food and were monitored daily by the same personnel for the duration of the experiment.

2.14.2 | Orthotopic xenograft model of Kcl-22

Female NSG mice (n = 3 mice per group) were intravenously inoculated with 5×10^6 Kcl-22 cells via tail-vein, using a 30-gauge insulin needle. Cells were administered as a suspension in phosphate-buffered saline at a concentration of 5×10^7 cells/mL. Mice (n = 3) were dosed for 20 days b.i.d, with 20 mg/Kg nilotinib (Novartis Pharma), starting day seven from injection of leukemic cells. The nilotinib solution (0.5% of HPMC and 0.05% of Tween 80 in water) was administrated orally (4 mg/mL) using a Teflon coated needle. Control mice received a similar volume of vehicle. All animals were observed thrice weekly for anemia, dehydration, and weight loss. Fluorescence imaging was used to determine the degree of infiltration with leukemic cells, 30 days after injection. For near infrared time-domain imaging,[57] a cocktail of 3 different fluorescently labeled monoclonal antibodies (CD45, CD13, and HLA-ABC) was administrated to each animal via tail-vein, 24 hours prior to imaging, in a total concentration of 1 μg/g. Briefly, mice were anesthetized with Isoflurane (Isoba Vet 3%, Intervet), depilated and whole-body imaging was performed with an Optix MX3 Small Animal Molecular Imager (ART Inc., Saint-Laurent, QC, Canada). All images were acquired with Optix Optiview (ART Inc.) acquisition software (version 2.00) and analyzed using Optix Optiview (version 2.02.00, ART Inc.).

2.14.3 | Subcutaneous xenograft model of Kcl-22

NSG mice (n = 5) were subcutaneously injected in the left flank area with 5×10^6 Kcl-22(memGFP) cells in 100 μL solution of PBS containing 10% of Matrigel (BD Matrigel Basement Membrane Matrix, BD Biosciences). The health status and weight of the mice were monitored daily. When tumor volumes reached 180-350 mm^3 (day 12), the mice were divided into two groups and treated orally q.d. for five days with either nilotinib 10 mg/kg or control, injections of 0.5% of HPMC and 0.05% of Tween 80 in water solution once daily. Tumor volumes were measured every second day by a digital caliper using the ellipsoid volume formula: Volume = π (length × width × height)/6. Non-fixed live tumors were sliced into 100 μm thick slices using the motorized vibroslicer NVSLM1 (WPI) and added in an IBIDI 8 μ-well in IMDM medium before microscopy. For SEM samples, whole tumors were placed in 15 mL tubes and fixed in 4% of PFA at 4°C over night before prepared for SEM as described above for Kcl-22 cells on coverslips.

2.15 | Statistical analysis

Differences between two groups were analyzed by two-tailed unpaired *t* test using GraphPad Prism 6 Version 6.03. *F* test was performed to verify that the internal variance in the groups were not significant. Significant difference was considered by a *P*-value < .05. For multiple comparisons of the effect of TKIs, a two-way ANOVA with Dunnett's multiple comparisons test was used. One-way ANOVA with Tykey's multiple comparisons test was used for investigation of significant changes in the Ba/F3 cells. For cell area and cell movement, unpaired Mann-Whitney tests were performed.

3 | RESULTS

3.1 | Effects of tyrosine kinase inhibitors (TKIs) on TNT formation in CML cell lines

In order to study the presence of TNTs in the CML cell lines K562 and Kcl-22, they were stably transduced to express cellular membrane localized GFP (memGFP) and cultured with and without drug treatment on fibronectin coated surfaces. To investigate the effects of TKIs on TNT formation, the K562 and Kcl-22 cells were treated with pre-apoptotic concentrations of imatinib, nilotinib, bosutinib, ponatinib, or dasatinib (Figure 1A), kinase inhibitors currently in use as CML therapy.[58] TNT quantification was performed as earlier described for acute myeloid leukemia (AML) cells.[31] The K562 and Kcl-22 cells formed very low numbers of TNTs without treatment (Figure 1A), however, 24 hours imatinib treatment resulted in a significant increase in TNT formation in both K562 (2.67 to 8.5 TNTs/100 cells, *P*-value <.001) and Kcl-22 cells (0.16 to 5.67 TNTs/100 cells *P*-value < .001) (Figure 1A). TNT formation following treatment with nilotinib, bosutinib, ponatinib, or dasatinib caused a variable TNT response between the K562 and Kcl-22 cell lines (Figure 1A). Nilotinib treatment increased TNT formation in Kcl-22 cells only (0.16 to 5.5 TNTs/100 cells, *P*-value < .001) while ponatinib significantly increased TNT formation in K562 cells only (2.67 to 7.5 TNTs/100 cells, *P*-value < .001). Interestingly, neither bosutinib nor dasatinib induced a significant increase in TNT formation in K562 or Kcl-22 cells (Figure 1A). A closer examination of K562 cells after imatinib treatment by scanning

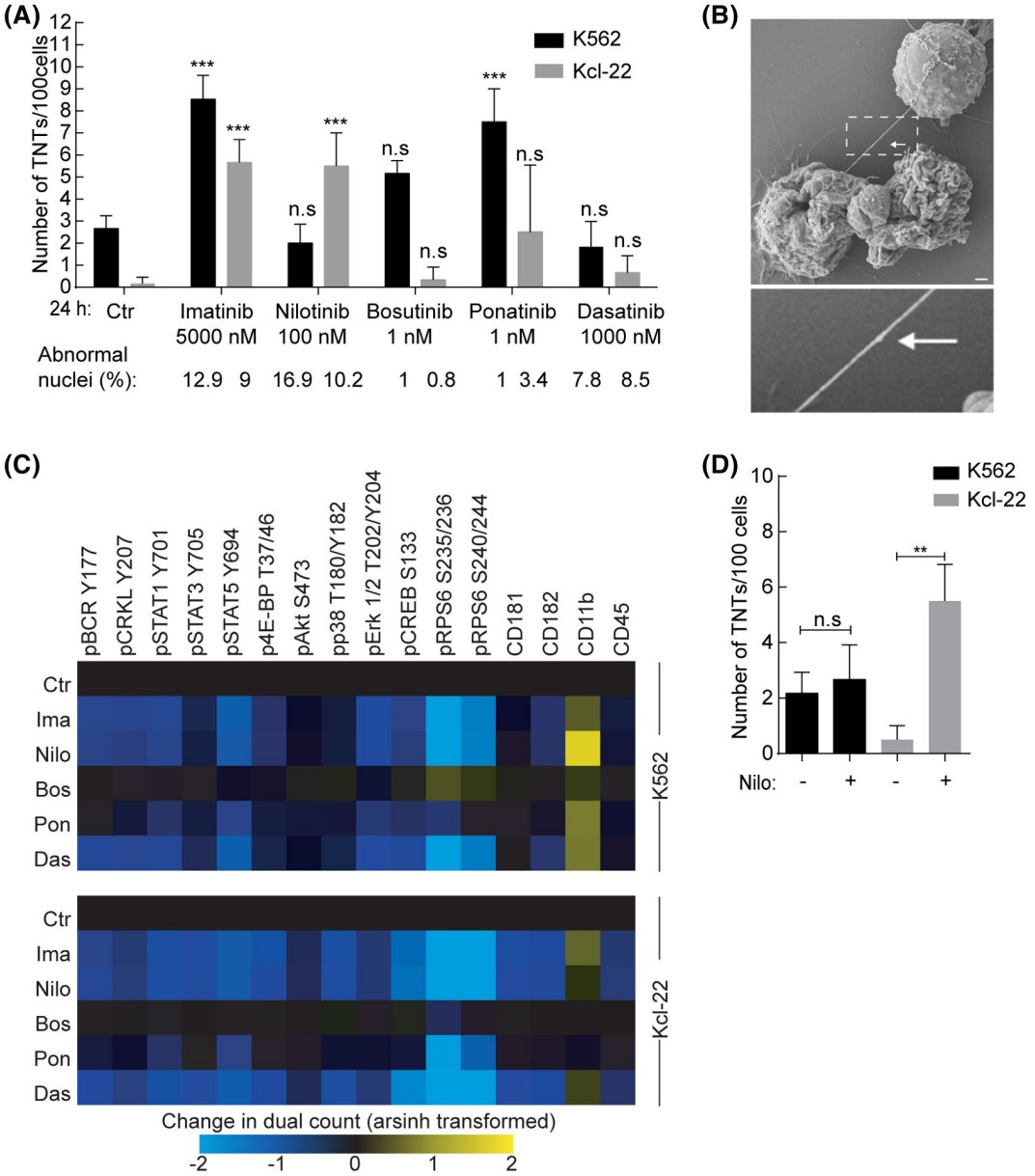

FIGURE 1 Effect of TKIs on TNT formation and intracellular signaling in CML cell lines. A, Kcl-22(memGFP) and K562(memGFP) cells were untreated (Ctr) or treated with 5000 nM imatinib, 1000 nM dasatinib, 100 nM nilotinib, 1 nM ponatinib, and 1 nM bosutinib for 24 hours. Percentage abnormal nuclei relative to Ctr cells calculated from Hoechst 33342 staining and manual counting is shown below. B, Scanning electron microscopy (SEM) image of a TNT connecting K562 cells that had been treated with 5000 nM imatinib for 24 hours. Jeol JSM-7400F LEI 4.0kV X3,700 WD 8.0 mm, scale bar = 1 μm. C, Mass cytometry analysis of down-stream signaling pathways of BCR-ABL1 in K562 and Kcl-22 cells treated with the TKIs as described in (A). Results are illustrated by fold changes relative to control (all gated for live cells) based on calculated Arcsinh Ratio of Medians, median from three independent experiments are shown. D, K562(memGFP) and Kcl-22(memGFP) cells were untreated (Ctr) or treated with 100 nM nilotinib (Nilo) for 1 hour. For all displayed graphs: Mean ±standard deviation (S.D.) used together with a two-way ANOVA with Dunnett's multiple comparison for (A) and unpaired *t* tests for (D) (***$P < .001$, **$P < .005$, n.s = not significant). All TNT quantifications were performed at least three independent times unless otherwise noted. Fluorescence microscopy was performed by the use of Zeiss AxioObserver Z1 fluorescence microscope with Alpha Plan Apochromat 63X/1.4 NA Oil DICIII and Zeiss Axio Observer A1with LD Plan Neofluar 20X/0.4 Corr Ph2

electron microscopy showed thin TNT structures (Figure 1B). To evaluate if the effect of TKIs on intracellular signal transduction targets could provide an explanation with respect to the heterogeneous dynamics of TNT formation in K562 and Kcl-22 cells, both cell lines were treated with the various TKIs for 24 hours and known alterations in central signaling pathways known to be downstream of BCR-ABL1[59] were analyzed using mass cytometry.[60] As expected after TKI treatment, we observed a marked reduction in phosphorylation of several ABL1 downstream signaling targets including

CrKL-(Tyr207), STAT5-(Tyr694) and RPS6 (Ser235/236 and Ser240/244) (Figure 1C). Also, phosphorylation of p38-(Thr180/Tyr182) and STAT3-(Tyr705) were reduced in the two cell lines, but there were no obvious differences in therapy response in the proteins investigated that could provide insight to the observed heterogenous dynamics of TNT formation in K562 and Kcl-22 following nilotinib treatment. Treatment with imatinib or nilotinib in both cell lines induced almost identical changes in the studied signal transduction phospho-proteins but differed in TNT formation following nilotinib treatment. This was also compared following one-hour treatment with pre-apoptotic concentration of nilotinib. Similar to 24 hours treatment a significant increase in TNT formation was observed in the Kcl-22 cell lines not found for the K562 cells (Figure 1D).

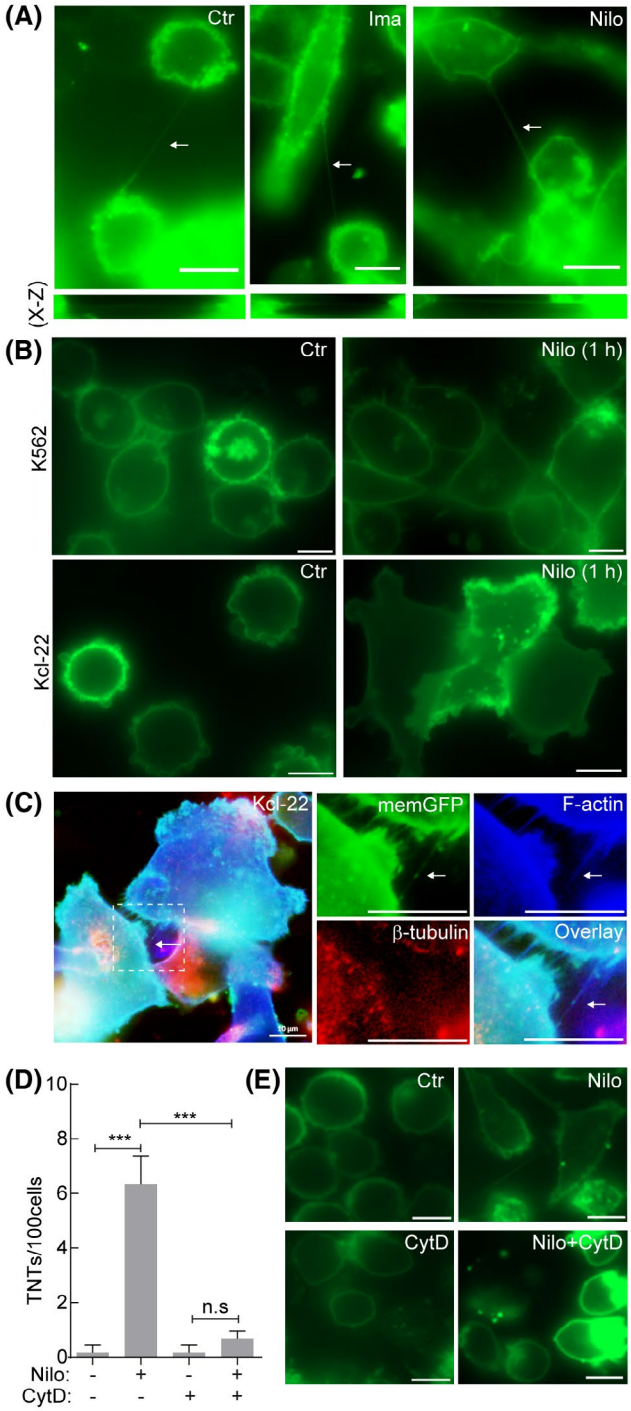

FIGURE 2 TNT increases following nilotinib treatment in actin dependent manner. A, Z-stack of TNTs connecting Kcl-22(memGFP) cells untreated (Ctr) or treated with nilotinib (Nilo, 100 nM) or imatinib (Ima, 5000 nM) for 24 hours. X-Z projection obtained from ImageJ are shown below. B, Fluorescence microscopy of K562(memGFP) and Kcl-22(memGFP) cells untreated (Ctr) or treated with nilotinib (Nilo, 100 nM) for 1 hours. C, Kcl-22(memGFP) cells were treated with nilotinib (Nilo, 100 nM) for 1 hours, fixed and stained with phalloidin (F-actin) AF350 followed by anti-β-tubulin staining. Representative images of three independent experiments are shown. D, Kcl-22(memGFP) cells were untreated or treated with nilotinib (Nilo, 100 nM) for 24 hours and TNT quantification was performed before and after addition of cytochalasinD (CytD, 2 μM) for 20 minutes, at 37°C. E, Representative fluorescence images from three independent experiments performed in duplicate of Kcl-22(memGFP) cells with no treatment (Ctr) or treatment with nilotinib (Nilo, 100 nM), cytochalasin D (CytD, 2 μM), or nilotinib (Nilo, 100 nM) followed by cytochalasin D (CytD, 2 μM). For all displayed graphs: Mean ± standard deviation (S.D.) used together with unpaired *t* tests (**$P < .005$, ***$P < .001$, n.s = not significant). All TNT quantifications were performed at least three independent times. Fluorescence microscopy was performed by the use of Zeiss AxioObserver Z1 fluorescence microscope with Alpha Plan Apochromat 63X/1.4 NA Oil DICIII. Scale bars = 10 μm

3.2 | The TNTs formed after nilotinib treatment contains actin

The TNT structures connecting the Kcl-22 cells both without any treatment and after treatment with imatinib or nilotinib, were verified not to be in contact with the substratum by z-stack imaging (x,z) (Figure 2A). In all experiments including Kcl-22 treated with nilotinib for 1 or 24 hours treatment, we observed a dramatic change in cell morphology from spherical semi-attached cells to firmly attached fibroblast-like cells, which was less evident in K562 cells (Figure 2B). The TNTs formed in nilotinib-treated Kcl-22 cells were further verified by immunofluorescence for the presence of F-actin and absence of β-tubulin (Figure 2C). The importance of F-actin in the TNT structures was next examined by treatment with the actin polymerization inhibitor cytochalasin D (CytD).[18,61] Kcl-22 cells were treated for 24 hours with nilotinib and quantified for TNTs before treatment with CytD for 20 minutes followed by a second TNT quantification (Figure 2D). This demonstrated that CytD blocked TNT formation in nilotinib treated cells and, interestingly fluorescent imaging showed less prominent change in cell morphology after nilotinib treatment (Figure 2E).

3.3 | IFNα increases TNT formation and membrane exchange in Kcl-22 cells

Since IFNα has been reported to increase adhesion of CML progenitor cells to bone marrow stromal cells and fibronectin coated surfaces,[46,48] it was of interest to investigate the effect of IFNα on TNT formation in K562 and Kcl-22 cells. Following treatment for 24 hours, TNT formation was significantly increased in Kcl-22 cells (0.8 TNTs/100 cells to 6.8 TNTs/100 cells, P-value < .005) compared to K562 cells (3.8 TNTs/100 cells to 2.3 TNTs/100 cells) (Figure 3A), similar to that observed after nilotinib treatment.

Interestingly, time-lapse microscopy of Kcl-22 cells following 1 hour treatment with IFNα visualized GFP positive objects moving along the TNTs, from one cell to another, indicating functional properties of the TNTs in Kcl-22 cells (Figure 3B and Supplemental Video S1). To further investigate, membrane and/or mitochondria exchange following IFNα treatment, a coculture of Kcl-22(memCherry) and Kcl-22(mitoGFP) was established. TNTs were observed connecting the memCherry and mitoGFP positive cells (Figure 3C) and a significant increase in memCherry positive membrane parts present in Kcl-22(mitoGFP) cells were observed, while no mitochondria in form of mitoGFP was observed in any of the mem-Cherry positive cells (Figure 3D,E, P-value < .005 and data not shown).

3.4 | Expression of BCR-ABL1 in Ba/F3 cells results in cell rounding

Since imatinib increased TNT formation in the BCR-ABL1 positive cell lines K562 and Kcl-22, we further investigated the role of BCR-ABL1 in the formation of TNTs. For this purpose, we utilized the murine pro B cell line Ba/F3. The Ba/F3 cells represent a well explored system for characterization of the oncogene function of BCR-ABL1, where expression of BCR-ABL1 allows Ba/F3 cells to proliferate independent of IL-3.[62] A doxycycline (dox) inducible BCR-ABL1 protein system was introduced in the Ba/F3 cells by electroporation and puromycin selection and was compared with an empty vector control (E.V.).[63] The induction of BCR-ABL1 expression by dox was verified by immunoblotting and IL-3-independent proliferation (Figure 4A,B). To visualize membranes and TNT formation, the cells were stained with WGA-488 before live cell fluorescence microscopy. In the Ba/F3 cells, dox-induced BCR-ABL1 expression resulted in a change from mostly semi-adherent and non-spherical morphology to spherical morphology with a reduced attachment to the fibronectin surface. In comparison, the imatinib treated BCR-ABL1 expressing cells displayed no change in cell morphology compared to the BCR-ABL1 induced control cells (Figure 4C). Interestingly, expression of BCR-ABL1 was accompanied by a tendency of reduced TNT formation, although not significant (Figure 4D). This was not due to the dox treatment, since dox treatment of Ba/F3 control cells (E.V.) resulted in an increase of TNT formation (Figure 4D). Increase in TNT formation after imatinib treatment was only present in the Ba/F3 cells not expressing BCR-ABL1. When BCR-ABL1 expression was induced, TNT numbers were decreased following imatinib treatment (Figure 4D). TNT structures were imaged in the Ba/F3 cells expressing the empty vector (E.V.) or doxycycline inducible BCR-ABL1 at basal level and treated with doxycycline (Figure 4E).

3.5 | TNT formation and increased cell surface adhesion by drug treatment

Cell adherence to fibronectin has previously been found to correlate with TNT formation[30] and treatment of CML cells with IFNα and TKIs have been shown to increase cell adherence to fibronectin, described through a restoration of the β1 integrin by IFNα.[46,48,64,65] To study the role of β1 integrin in cell adherence and TNT formation, we pre-incubated Kcl-22 cells for 30 min with a β1 integrin blocking antibody before treatment for one hour with either IFNα (100 U/mL) or nilotinib (1 μM). The Kcl-22 cells, without pre-incubation with the β1 integrin blocking antibody (Ctr), showed transformed cell morphology and significantly increased cell surface area on the fibronectin coated surface following nilotinib treatment, whereas IFNα treatment resulted in altered morphology only without significant changes in cell surface area (Figure 5A,B). Strikingly, these cell morphology changes after nilotinib and IFNα treatment were completely abolished by pre-incubation with the β1 integrin blocking antibody (Figure 5A,B). In support of this, cell movement was investigated by time-lapse microscopy, where the images were acquired every 10th second for a total 2 min for each duplicate, demonstrating that the IFNα and nilotinib-induced changes in cell morphology was followed with a decrease in cell movement (Figure 5C,D and Supplemental videos 2-7). Conversely, pre-treatment with the β1 blocking antibody resulted in increased cell movement (representative videos shown in Supplemental videos 2-7). These observed changes were quantified by tracking the distance of movement by the cells in the time lapse-videos and resulted in significant increase in distance when cells were treated with β1 integrin blocking antibody (Figure 5C,D).

3.6 | Nilotinib treatment in a subcutaneous Kcl-22 mouse model causes cellular morphology changes

Initially the efficacy of nilotinib was investigated in an orthotopic xenograft mouse model of Kcl-22. Fluorescence

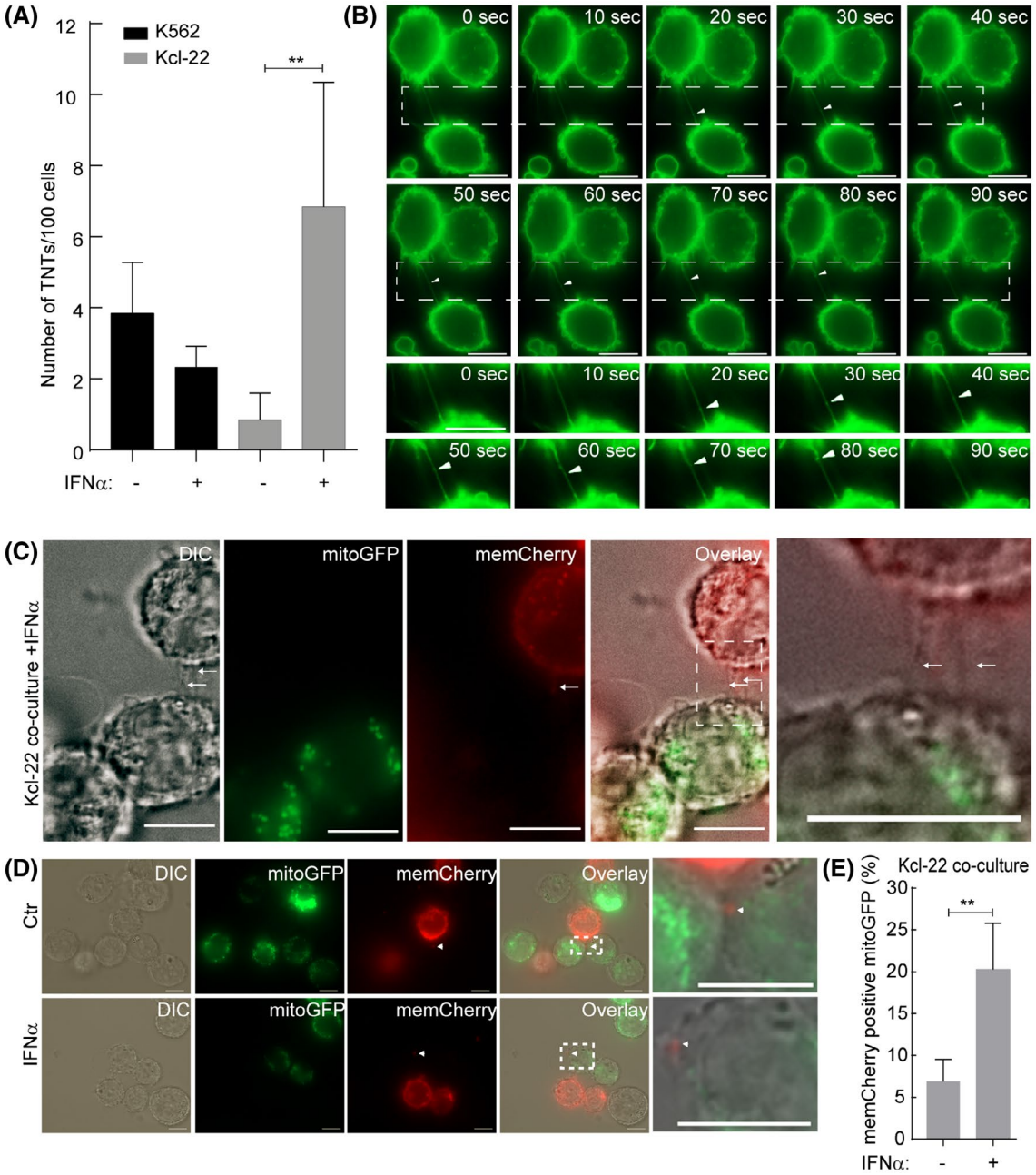

FIGURE 3 IFNα treatment increases TNT formation and membrane exchange in Kcl-22 cells. A, Number of TNTs were quantified in K562(memGFP) and Kcl-22(memGFP) cells treated with interferon-α (IFNα, 100 U/mL) (+) for 24 hours compared to untreated (−). B, Time-lapse of Kcl-22(memGFP) cells treated with IFNα (100 U/mL) for 1 hour where images were captured every 10th second for a total of 120 seconds. Arrow heads indicate movement of memGFP along the TNT structure over time. C, Coculture of Kcl-22(memCherry) (35 000 cells) and Kcl-22(mitoGFP cells) (35 000 cells) treated with IFNα (100 U/mL) for 24 hours. Arrows indicate TNT connection between the two cell lines. D, Red dots indicated by arrowheads demonstrate memCherry transferred from Kcl-22(memCherry) cells to Kcl-22(mitoGFP) cells in untreated control cells and IFNα treated cells. E, Significant presence of memCherry in Kcl-22(mitoGFP) cells after 24 hours coculture and IFNα treatment. Experiments were performed in duplicates and repeated in two independent experiments. A total of 189 cells were included in the control while 196 cells where counted in the IFNα treatment. Scale bar = 10 μm. For all displayed graphs: Mean ± standard deviation (S.D.) used together with unpaired *t* tests (**$P < .005$, n.s = not significant). All TNT quantifications were performed at least three independent times unless otherwise noted. Fluorescence microscopy was performed by the use of Zeiss AxioObserver Z1 fluorescence microscope with Alpha Plan Apochromat 63X/1.4 NA Oil DICIII

imaging of mice treated per oral for 20 days with nilotinib (10 mg/kg, b.i.d.) starting at day 7, showed great efficacy of the treatment at day 30 compared to the control vehicle (0.5% of hydroxypropyl methylcellulose (HPMC) and 0.05% of Tween 80 in water solution) treated mice and infiltration of leukemic cells was visible only in the superficial lymph

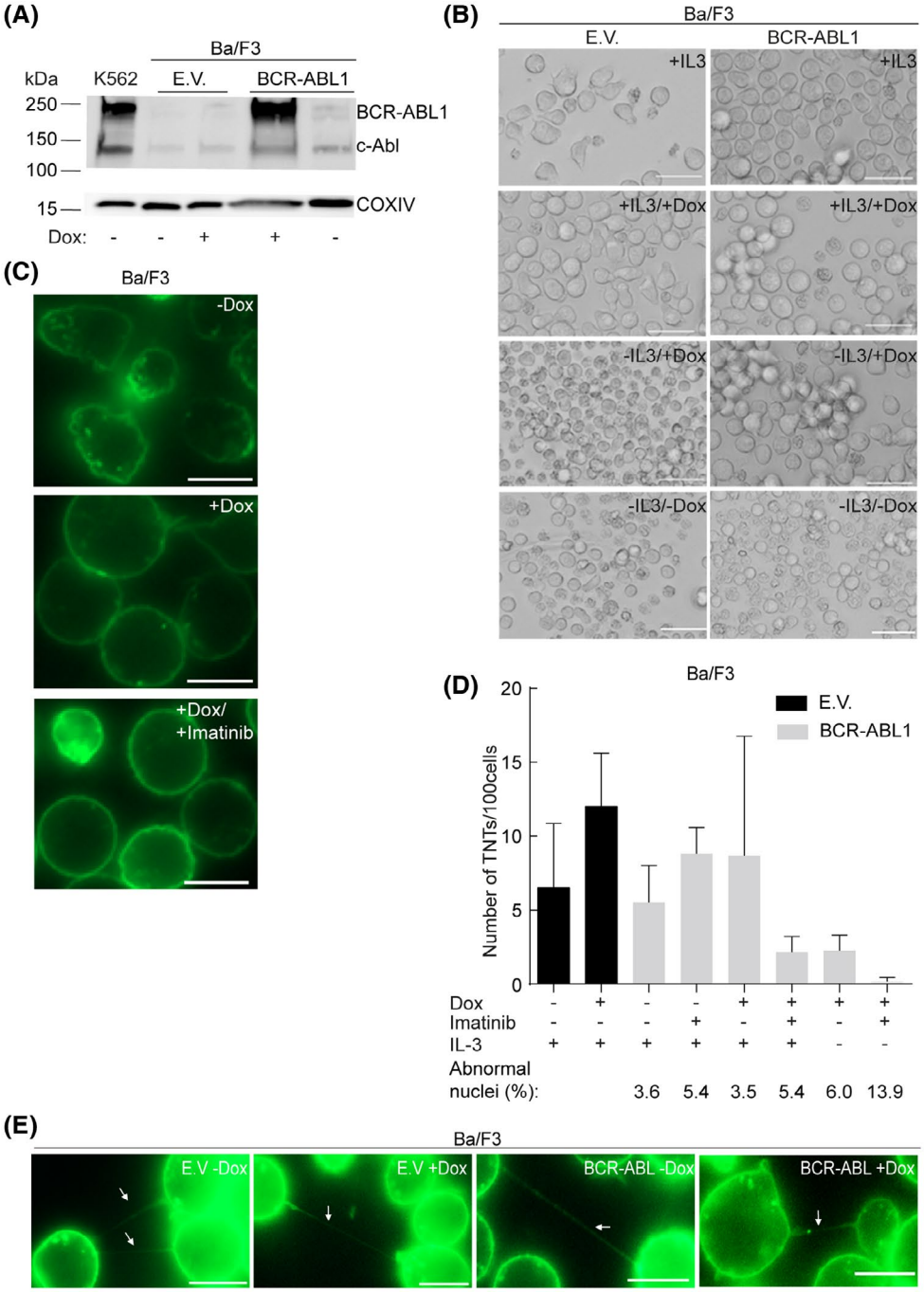

FIGURE 4 Effects of BCR-ABL1 expression on TNT formation and cell morphology in Ba/F3 cells. A, Ba/F3 cells transfected with empty vector (E.V.) or BCR-ABL1 were untreated (−) or treated (+) with doxycycline (0.1 μM) for 24 hours, lysed and immunoblotted using anti-c-Abl antibody to verify BCR-ABL1 expression. K562 cells were used as positive control for BCR-ABL1 expression and COXIV as loading control. B, Validation of IL-3 independence following BCR-ABL1 expression. Representative images captured by phase/contrast light microscopy. Scale bars = 10 μm. C, Fluorescence microscopy images of Ba/F3-BCR-ABL1 doxycycline inducible cells cultured in the presence or absence of IL-3 and without (−Dox) or with doxycycline (+Dox, 0.1 μM) stained with WGA-488. Scale bars = 10 μm. D, TNT quantification of Ba/F3-E.V. and Ba/F3-BCR-ABL1 cells cultured in the presence (+) or absence (−) of IL-3 with (+) or without (−) doxycycline (+Dox, 0.1 μM), and with (+) or without (−) imatinib (Ima, 5000 nM). For selection, 1 μg/mL puromycin was present in the culture media in all conditions. Percentage abnormal nuclei relative to control following Hoechst 33342 staining is shown below. E, Fluorescence microscopy of Ba/F3-E.V. or Ba/F3-BCR-ABL cells with doxocycline (+Dox) or without (−Dox). Cells were stained with WGA-488. Arrow heads indicate TNT connections. Scale bar = 10 μm. Microscopy was performed using Zeiss AxioObserver Z1 fluorescence microscope with Alpha Plan Apochromat 63X/1.4 NA Oil DICIII and Zeiss Axio Observer A1with LD Plan Neofluar 20X/0.4 Corr Ph2. All data are presented as mean ± standard deviation (S.D.) and investigated for significance by one-way ANOVA with Tykey's multiple comparisons test. All experiments were performed three times except TNT quantification of Ba/F3 treated with doxocycline and incubated without IL-3 (n = 2)

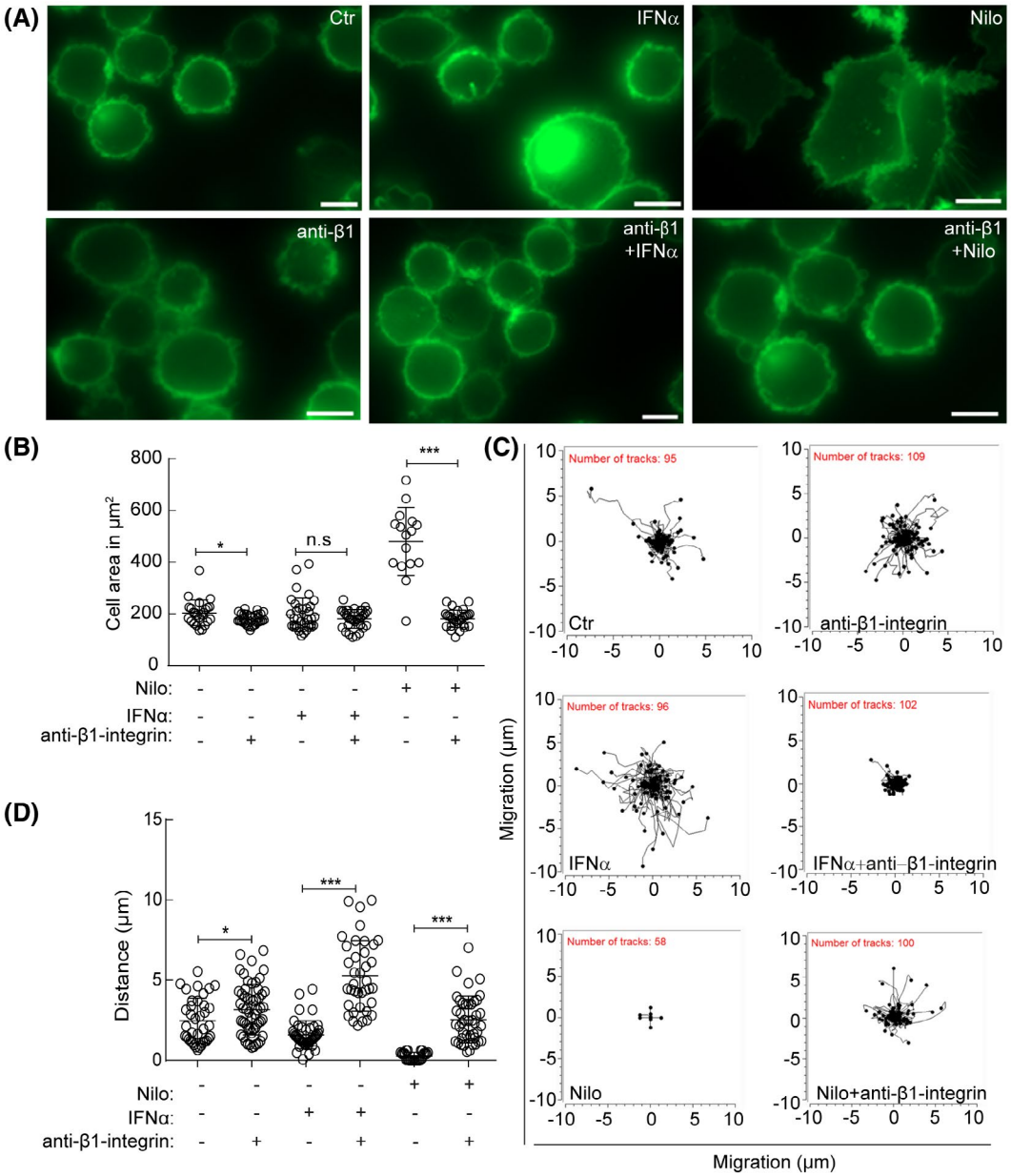

FIGURE 5 Adherence to fibronectin enhances TNT formation and reduces cell movement in Kcl-22 cells. A, Kcl-22(memGFP) cells were pre-treated for 30 minutes with anti-β1 integrin blocking antibody (10 μg/mL) before seeded onto fibronectin-coated IBIDI wells, allowed to adhere for 3 hours before treated for 1 hour with IFNα (100 U/mL) or nilotinib (Nilo, 1 μM) (lower panel). This was compared to cells not pre-treated with anti-β integrin blocking antibody (upper panel). Cells were investigated by fluorescence microscopy. Scale bars = 10 μm. B, Cell area (μm^2) of experiments in (A) was measured manually using ImageJ. C, Cells seeded on fibronectin were tracked for migration (μm) by live cell imaging and analyzed using metamorph and measurements were calculated using Chemotaxis and Migration (IBIDI) plugin in ImageJ. D, Statistical analysis of migration of the Kcl-22(memGFP) cells following the different treatment conditions. Significance of changes was calculated using unpaired Mann-Whitney test. Mean ±standard deviation (S.D.) (*$P < .05$, ***$P < .001$, n.s = not significant). Results are presented as mean ±standard deviation (S.D.) and significance investigated by the use of unpaired *t* tests (***$P < .001$, n.s = not significant). Microscopy was performed using Zeiss AxioObserver Z1 fluorescence microscope with Alpha Plan Apochromat 63X/1.4 NA Oil DICIII

nodes and gastrointestinal tract of the untreated mice (Figure 6A,B). The treatment was well tolerated since no changes in weight were observed between mice treated with nilotinib and controls (Figure 6C). Efficacy of treatment was also confirmed by survival where the control mice had a median survival of 34 days, while the treated animals lived disease free for more than 90 days (Figure 6D).

In further attempts to examine TKI modulations of TNTs and cell morphology in vivo, we compared Kcl-22(memGFP) cells derived from a subcutaneous mouse model following

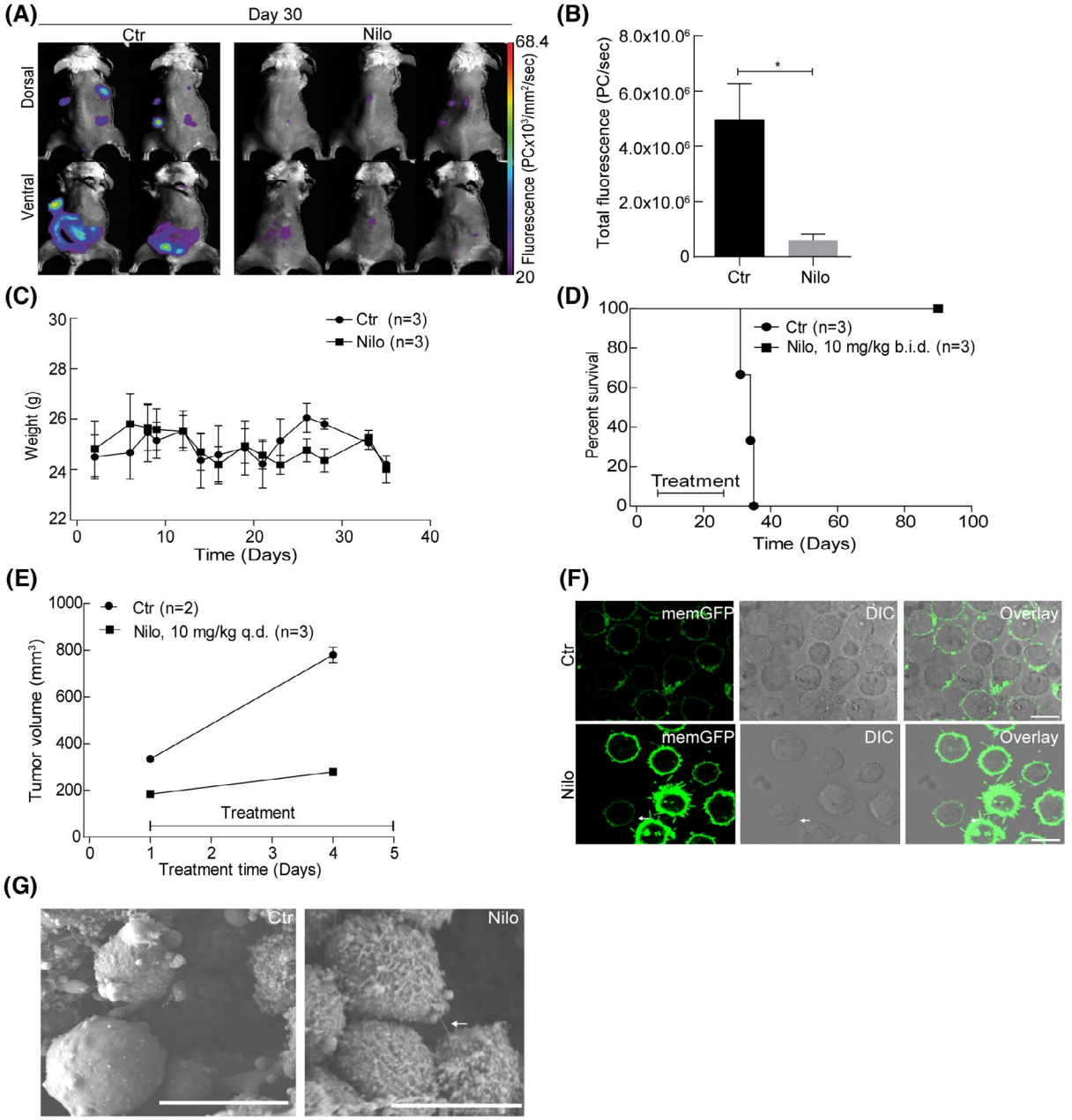

FIGURE 6 In vivo effect of nilotinib on Kcl-22 cells in a subcutaneous xenograft tumor model. A, Time-domain fluorescence imaging results for mice injected i.v. with Kcl-22 cells. Vehicle (Ctr) treated mice (two mice imaged) versus mice treated with nilotinib (Nilo, 20 mg/kg b.i.d. per oral) for 20 days with start day 7. Superficial lymph nodes and gastro-intestinal (G.I.) tract infiltration are visible in the control group, while the treated mice present only background fluorescence. i.v: intravenously, b.i.d: twice daily, PC: photon counts. B, Fluorescence quantification (PC/sec) of (A) a significant reduction in nilotinib (Nilo) treated mice compared to vehicle (Ctr) treated (*$P < .05$). C, Weight changes in vehicle (Ctr) treated mice and nilotinib (Nilo) treated mice. D, Survival curves for vehicle (Ctr) treated mice and mice treated with nilotinib (Nilo) in the orthotopic Kcl-22 xenograft model. E, Five mice were injected subcutaneously with Kcl-22(memGFP) cells and matrigel. At day 12, three mice with similar tumor size (average of 184 mm^3) were treated once per day for 5 days with nilotinib (Nilo, 10 mg/kg) and two mice with similar size tumors (average of 334 mm^3) were vehicle (Ctr) treated. Tumor volumes were measured at day 1 and day 4. At day 5, the mice were treated 1 hour prior to euthanization and collection of tumors. F, Live tumor sections (100 μm) were performed by the use of Vibroslice and tumor derived memGFP positive cells from nilotinib (Nilo) and vehicle (Ctr) treated mice were investigated by confocal microscopy using the Leica TCS SP5 confocal microscope with the resonant scanner and the 63×/1.40 NA oil-immersion objective. Scale bar = 10 μm. G) Tumor sections (100 μm) from nilotinib (Nilo) and vehicle (Ctr) treated mice were fixed, prepared for and analyzed by scanning electron microscopy Jeol JSM-7400F LEI 4.0kV X3, 700 WD 8.0 mm. Scale bar = 1 μm. For all: Mean ± standard deviation (S.D.) is demonstrated in the graphs and significance investigated by the use of unpaired *t* test

treatment with and without nilotinib. At day 12 after injection with Kcl-22(memGFP) cells three mice with similar tumor volumes (average tumor volume 184 mm^3) and two mice with similar volumes (average tumor volume 335 mm^3) were treated per oral with nilotinib (10 mg/kg g.d.) or vehicle control (0.5% of HPMC and 0.05% of Tween 80 in water solution) for 5 days (Figure 6E). On day 5 of treatment, tumors were collected one hour after nilotinib and vehicle administration. Confocal fluorescence microscopy of non-fixed live vibratome sliced tumor sections indicated increased number of TNT-like structures in the tumors from the nilotinib treated mice as compared to vehicle treated mice (Figure 6F). When the cells retrieved from the tumors were examined by scanning electron microscopy (SEM), a difference in cell morphology and TNT-like structures was evident in the tumors from untreated and nilotinib treated mice (Figure 6G).

3.7 | TKI or IFNα treatment of CML chronic phase derived bone marrow patient cells do not result in morphology changes or increased number of TNTs

To characterize the basal level of TNTs on primary CML cells, fresh bone marrow cells from four chronic phase CML patients were stained with WGA-594 and examined by live microscopy (Samples 1-4, Supplemental Table 1). Similar to the CML cell lines, these cells formed few or no TNTs (Supplemental Figure 1A). To further examine the effect of TKIs or IFNα treatment on primary patient derived cells, cryopreserved bone marrow-derived cells from six chronic phase CML patients and three healthy donors were thawed (Samples 5-13, Supplemental Table 1) and these cells were treated with nilotinib (1 μM), IFNα (100 U/mL) or imatinib (5 μM) for 24 hours before examined for morphological changes and TNT formation compared to untreated cells. In these cells, no changes in morphology or movement were observed in the CML patient-derived or healthy cells after nilotinib or IFNα treatment and no or few TNTs were observed (Supplemental Figure 1B-D). Following this, we aimed to purify hematopoietic progenitor cells by the use of negative selection using (EasySep Human progenitor cell Enrichment Kit, magnetic beads coated with antibodies targeting non-progenitor cells with CD2, CD3, CD14, CD16, CD19, CD24, CD66b, glycophorin A) for three CML patient samples and one healthy bone marrow sample. The negative selected and positive selected cells were treated with nilotinib (1 μM) and if sufficient number of cells, with IFNα (100 U/mL) for 24 hours, however; no changes in morphology or reduced mobility were found for either the negative or positive sorted cells and few or no TNTs (Supplemental Figure 1E). The CML patient cells, including two positive sorted samples (Samples 6 and 7), and one healthy bone marrow sample (negative control) were analyzed by FISH for reverification of BCR-ABL1 showing that BCR-ABL1 was expressed in both the total bone marrow sample as well as in the positive sorted cells, whereas the healthy bone marrow sample was negative for BCR-ABL1 (Supplemental Figure 1F).

4 | DISCUSSION

TNTs are highly dynamic intercellular communication structures consisting of plasma membrane and F-actin, however, the detailed understanding of TNT regulatory mechanisms are still limited.[66-68] Since the tyrosine kinase ABL1 and the oncogenic fusion protein BCR-ABL1 include distinct F- and G-actin binding domains with actin bundling activity,[69] we examined various BCR-ABL1 expressing cells with respect to TNT formation. BCR-ABL1 positive CML cells, cell lines, and patient-derived cells, displayed limited numbers or absence of TNT formation compared to acute myeloid leukemia cells, stromal cells and other cancer cells.[30,31,41,70,71] TNT formation between cells in vitro is highly dependent on adherence, and culturing leukocytes on a supportive layer of mesenchymal stem cells (MSCs) or fibronectin increases TNT formation.[30,72] The limited TNT numbers observed in our study is supported by Kolba and coworkers also reporting limited TNTs formed by K562 cells[43] and this could be related to the observation that primary CML cells have adhesion defects and thus adhere poorly to bone marrow stroma,[9] which consequently may result in a lack of TNT formation and cellular communication.

Interestingly, we find both increased adhesion and a change in morphology in the CML cell line Kcl-22 following treatment with imatinib, nilotinib, or IFNα accompanied by a significant increase in TNT formation (Figures 1A, 2A,B, and 3A). IFNα was the first effective CML therapy and is now re-evaluated in combination with TKIs for more rapid disease control and possibly cure.[49,73] One of the proposed mechanisms for the efficacy of IFNα in treatment of CML patients is indeed through restored adhesion of CML cells to the bone marrow stroma.[74] Similarly, TKI treatment has been reported to increase CML cell adherence to fibronectin.[64] Together, these observations suggest that increased adherence of CML cells could play a role in treatment of CML patients. The functionality of the IFNα-enhanced TNTs was examined by live-cell microscopy where memGFP were found to be transported between Kcl-22 cells, suggesting that the TNTs formed after IFNα treatment could be functional as transportation devices. This transport was further investigated by coculturing Kcl-22 cells(mitoGFP) and Kcl-22(memCherry) following treatment with IFNα where these cells were connected by TNTs and memCherry was significantly increased in the Kcl-22(mitoGFP) cells (Figure 3C-E). This could be explained by other means of transportation or cell-to-cell

communication besides TNT formation, but TNTs could play an important role in IFNα induced cell-to-cell communication, possible also involving the bone marrow microenvironment as demonstrated by Kolba and coworkers.[43]

In order to search for a possible link between TNT, BCR-ABL1, and actin, we studied the activity of the three GTPases Rac1, Rho, and Cdc42 by the use of a pull-down and activity detection in K562 and Kcl-22 cells (data not shown). However, we did not find that the treatment resulted in changes in the GTPase activity of these three GTPases. A reduction in the total protein of the Rac1 guanine exchange factor (GEF) protein Tiam-1 was found following imatinib and nilotinib treatment in the Kcl-22 cells, but not in the K562 cells (data not shown). Elevated levels of Tiam-1 have been associated with increased migration and metastasis in colon tumor cells.[75] In our hands, no consistent G-protein modulation could explain the nilotinib TNT-response in the Kcl-22 cells, or the similar imatinib TNT-response observed in both Kcl-22 and K562. However, we cannot rule out that similar modulation of related GTPases may explain the difference in nilotinib response between Kcl-22 and K562 cells.

Since IFNα do not specifically inhibit the tyrosine kinase activity of BCR-ABL1 like the TKIs, but rather provide distinct cellular signaling and immune responses toward the leukemic cells this could indicate that the TNT formation is independent of direct BCR-ABL1 signaling.[76,77] To investigate the involvement of BCR-ABL1 in TNT formation, we used a doxycycline-inducible BCR-ABL1 Ba/F3 cell system. BCR-ABL1 induction resulted in increased cell rounding compared to the Ba/F3 control cells (Figure 4C). Since imatinib treatment did not cause an increase in TNT formation in BCR-ABL1 expressing Ba/F3 cells, but rather in the Ba/F3 cells alone, this suggest that the TNT increase most likely involves other factors besides the inhibition of BCR-ABL1. This was also supported by the comparison of intracellular signaling by mass cytometry, where known BCR-ABL1 downstream targets like phospho-STAT-5 and phospho-CrkL [78] were down-regulated by the TKI treatments independently of the differences in TNT response observed. A similar inhibition of phosphorylated STAT-5 and CrkL were observed in both cell lines after imatinib and nilotinib treatment, even though both cell lines have significant more TNTs after imatinib treatment, while nilotinib only induced TNTs in the Kcl-22 cells (Figure 1A,C). Another down-stream BCR-ABL1 target, STAT3 has been suggested to play a role in BCR-ABL1 independent resistance in CML,[79] as well as in IL-10/STAT3 signaling dependent TNT formation in a subtype of anti-inflammatory macrophages in tuberculosis and HIV-1 coinfected patients.[22] However, in the Kcl-22 or K562 cells, the results from the STAT3 signaling in our experiments could not distinguish the changes in signaling observed between the TKIs causing an increase in TNT formation versus those that did not. Based on these observations, we suggest that TNT regulation is not modulated directly by BCR-ABL1 or its kinase activity, however, TNT formation may be modulated by altered cell morphology that is under control of ABL1 and BCR-ABL1 in selected cell types.

Since IFNα as well as nilotinib were able to increase TNT formation in Kcl-22 cells and IFNα previously have been shown to restore the ability of CML cells ability to bind to fibronectin through restoration of β1 integrin function, we examined β1 integrin as a common feature between the two therapies.[46] Indeed, we found that the change in morphology caused by nilotinib, measured by cellular size, were significantly lower when pre-incubated with a β1 integrin blocking antibody. Also, the induced cell adhesion by both IFNα and nilotinib seemed to involve β1 integrin by significantly increasing the average distance of cell movement when cells were pre-treated with the β1 integrin blocking antibody (Figure 5C,D). The Kcl-22 cells showed increased movement and more cellular rounding after pre-incubation with the β1 integrin blocking antibody (Figure 5A,C,D, Supplemental videos 2-7). Together with our observations in the Ba/F3 cells, this supports a hypothesis where CML cells adhering poorly to fibronectin results in cell rounding and subsequently a lower level of TNT formation. The importance of cell attachment to the given substrate and capability to form TNTs have previously been shown by others and supports our findings.[30] Strikingly, nilotinib treatment in a Kcl-22(memGFP) subcutaneous mouse model also caused a change in cellular morphology and appearance of TNT-like structures in the Kcl-22 cells (Figure 6F,G). This demonstrated that the morphological changes and TNT modulations found in vitro similarly was present in vivo.

When treating bone marrow cells obtained from patients with chronic phase CML with IFNα and nilotinib, no change in TNT numbers or cell morphology where observed (Supplemental Figure 1B-E). BCR-ABL1 expressing CML is a model of oncogene driven malignancy, but clearly chronic phase CML respond differently than blast crisis CML when treated with TKIs. Blast crisis CML patients need intensive chemotherapy combined with TKI to secure complete remission, before consolidation by hematopoietic stem cell transplantation and TKIs maintenance therapy to obtain long-term cure.[80] It has been shown that blast crisis CML has more mutations associated with myeloid malignancies than found in chronic phase CML, and that blast crisis cells contain higher level of BCR-ABL1 mRNA.[81] In vitro, primary chronic phase cells are not particularly sensitive to TKIs,[82] and therefore patient-derived blast crisis cells have been used in development of new kinase inhibitors for chronic phase CML.[83] Our study has examined the TKI effect in various CML models, and our observations on Kcl-22 and K562 cells could mostly be relevant for blast crisis CML. However, we hypothesize that various CML myeloid progenitors and more differentiated myeloid CML cells in chronic phase disease are involved in TNT formation in vivo under TKI and IFNα therapy, particularly since

the CML cells interacts with a wide repertoire of stromal and host cells at various anatomical locations.[11,84]

Chronic myeloid leukemia with its pathognomonic BCR-ABL1 fusion protein is one of several myeloid neoplastic diseases that originate from hematopoietic stem cells,[85,86] and in which the malignant cell has a close relation to mesenchymal support cells in the bone marrow. TNTs are proposed as one mechanism of interaction between mesenchymal stromal cells and leukemic cells in the leukemic stem cell niche.[29,68,87,88] Kolba and coworkers showed that stromal cells transferred vesicles through TNTs to K562 cells and that transfer of vesicles correlated with increased resistance toward imatinib treatment.[43] This underscores the importance of interaction between CML cells, mesenchymal stromal cells and the bone marrow niche, a system of cell-to-cell communication that include secreted factors, extracellular matrix interactions and direct cell-to-cell interactions.[89-93] This leukemic-mesenchymal interaction has led to models for leukemogenesis that involve bidirectional interactions.[94-96] Our data focus on inter-leukemic cell communication by TNT and likely this play a functional role since leukemic cells are found in niches and aggregates in the bone marrow. However, it is highly plausible that TNT formation related to CML cells play a more significant role with respect to cell-to-cell interaction with the numerous cell types in the bone marrow microenvironment as demonstrated by Kolba and coworkers.[43] We speculate that hibernating CML cells, only detected by sensitive BCR-ABL1 PCR of the bone marrow, through their TNT connections with stromal cells, may or may not cause relapse years after treatment.[97]

In conclusion, kinase inhibitors or IFNα-treatment resulted in increased numbers of TNTs in selected blast crisis CML derived cell lines and a similar result was found with TNT-like structures in an in vivo Kcl-22 subcutaneous mouse model following nilotinib treatment, but not in BCR-ABL1 expressing Ba/F3 cells or in BCR-ABL1 positive cells from chronic phase CML patients. The observed increase in TNTs through TKIs and IFNα appear to involve β1integrin dependent function and cell adhesion. This confirms that TNT formation is contextual to the complex regulation of cellular shape and adhesion. Therapeutic responses to TKIs and IFNα in CML may therefore be more dependent on tumor-stroma and cell-cell interactions than previously anticipated. A more complete understanding of TNT function in leukemogenesis and therapy resistance will likely require novel experimental technologies employed on disease models that reflect the pathophysiology of CML.

ACKNOWLEDGMENTS

We thank Dr. André Sulen (University of Bergen, Norway) for help with sorting of memGFP, memCherry, and mitoGFP cells, Dr. Manja Schubert (University of Bergen, Norway), for assistance in vibratome sectioning of subcutaneous tumors, Dr. Tatiana Karpova (NIH, USA) for assistance with the analysis of cell movement and Anne Karin Nyhaug and Endy Spriet (MIC, University of Bergen) for support with preparation and performing SEM analysis and Misbah Sabir for lymphoprep and biobanking of the bone marrow CML patient and healthy donor samples. The scanning electron microscopy and confocal imaging was performed at the Molecular Imaging Center, Dept. of Biomedicine, University of Bergen. The mass cytometry was performed at the Flow Cytometry Core Facility, Department of Clinical Science, University of Bergen. The Helios Mass Cytometer was funded by Bergen Forskningsstiftelse (Bergen Research Foundation), Trond Mohn Foundation. Calum Leitch (University of Bergen) and Dr. Genoveffa Franchini (NIH, USA) are acknowledged for helpful feedback on the manuscript. This study was supported by University of Bergen and the Intramural Research Program of the National Institutes of Health, National Cancer Institute, Center for Cancer Research, and federal funds from the National Cancer Institute, National Institutes of Health (MO), Norwegian Cancer Society with Solveig & Ole Lunds Legacy and Øyvinn Mølbach-Petersens Fond for Clinical Research (BTG), Melzer Høyskolefond (BTG), Bergen Forskningsstiftelse (Bergen Research Foundation), Trond Mohn Foundation (VA), Helse Vest RHF and Helse Bergen HF (project numbers 911809, 911852, 912171, 240222) (EM), Norwegian Cancer Society (205729) (EM), Norwegian Research Council of Norway through its Centers of excellence funding scheme, project number 223250 and 262652 (EM), the Norwegian Research Council Project Number 294916 (J.E.), the Norwegian Cancer Society Project Number 182524 (J.E.) and a partly support by the Research Council of Norway through its Centers of Excellence funding scheme, project number 262652 (J.E.).

CONFLICT OF INTEREST

The authors declare no conflicts of interests.

AUTHOR CONTRIBUTIONS

M. Omsland and V. Andresen designed and performed research, analyzed data and wrote paper, B.T. Gjertsen designed, collected patient material, analyzed data and wrote paper, S.E. Gullaksen, P. Ayuda-Durán, A. Brendehaug, R. Hovland and M. Popa performed research and wrote paper, J. Enserink and E. Mc Cormack, contributed with reagents, helped in analyzing data and wrote paper.

REFERENCES

1. CML Trialists' Collaborative Group, C. T. S. U., Radcliffe Infirmary, Oxford. Interferon alfa versus chemotherapy for chronic myeloid leukemia: a meta-analysis of seven randomized trials:

Chronic Myeloid Leukemia Trialists' collaborative group. *J Natl Cancer Inst*. 1997;89:1616-1620.
2. Gratwohl A, Baldomero H, Passweg J. Hematopoietic stem cell transplantation for hematological malignancies in Europe. *Leukemia*. 2003;17:941-959.
3. Talpaz M, Kantarjian HM, McCredie K, Trujillo JM, Keating MJ, Gutterman JU. Hematologic remission and cytogenetic improvement induced by recombinant human interferon alpha A in chronic myelogenous leukemia. *N Engl J Med*. 1986;314:1065-1069.
4. Talpaz M, Kantarjian HM, McCredie KB, Keating MJ, Trujillo J, Gutterman J. Clinical investigation of human alpha interferon in chronic myelogenous leukemia. *Blood*. 1987;69:1280-1288.
5. Simonsson B, Gedde-Dahl T, Markevarn B, et al. Combination of pegylated IFN-alpha2b with imatinib increases molecular response rates in patients with low- or intermediate-risk chronic myeloid leukemia. *Blood*. 2011;118:3228-3235.
6. Weisberg E, Manley PW, Breitenstein W, et al. Characterization of AMN107, a selective inhibitor of native and mutant Bcr-Abl. *Cancer Cell*. 2005;7:129-141.
7. Hochhaus A, Kreil S, Corbin AS, et al. Molecular and chromosomal mechanisms of resistance to imatinib (STI571) therapy. *Leukemia*. 2002;16:2190-2196.
8. Radich JP, Deininger M, Abboud CN, et al. Chronic myeloid leukemia, version 1.2019, NCCN clinical practice guidelines in oncology. *J Natl Compr Canc Netw*. 2018;16:1108-1135.
9. Gordon MY, Dowding CR, Riley GP, Goldman JM, Greaves MF. Altered adhesive interactions with marrow stroma of haematopoietic progenitor cells in chronic myeloid leukaemia. *Nature*. 1987;328:342-344.
10. Bhatia R, McGlave PB, Dewald GW, Blazar BR, Verfaillie CM. Abnormal function of the bone marrow microenvironment in chronic myelogenous leukemia: role of malignant stromal macrophages. *Blood*. 1995;85:3636-3645.
11. Perrotti D, Silvestri G, Stramucci L, Yu J, Trotta R. Cellular and molecular networks in chronic myeloid leukemia: the leukemic stem, progenitor and stromal cell interplay. *Curr Drug Targets*. 2017;18:377-388.
12. Hochhaus A, Larson RA, Guilhot F, et al. Long-term outcomes of imatinib treatment for chronic myeloid leukemia. *N Engl J Med*. 2017;376:917-927.
13. Bruck O, Blom S, Dufva O, et al. Immune cell contexture in the bone marrow tumor microenvironment impacts therapy response in CML. *Leukemia*. 2018;32:1643-1656.
14. Zhang B, Ho YW, Huang Q, et al. Altered microenvironmental regulation of leukemic and normal stem cells in chronic myelogenous leukemia. *Cancer Cell*. 2012;21:577-592.
15. Joyce JA, Pollard JW. Microenvironmental regulation of metastasis. *Nat Rev Cancer*. 2009;9:239-252.
16. Rustom A, Saffrich R, Markovic I, Walther P, Gerdes H-H. Nanotubular highways for intercellular organelle transport. *Science*. 2004;303:1007-1010.
17. Abounit S, Zurzolo C. Wiring through tunneling nanotubes-from electrical signals to organelle transfer. *J Cell Sci*. 2012;125:1089-1098.
18. Gurke S, Barroso JF, Hodneland E, Bukoreshtliev NV, Schlicker O, Gerdes HH. Tunneling nanotube (TNT)-like structures facilitate a constitutive, actomyosin-dependent exchange of endocytic organelles between normal rat kidney cells. *Exp Cell Res*. 2008;314:3669-3683.
19. Sowinski S, Jolly C, Berninghausen O, et al. Membrane nanotubes physically connect T cells over long distances presenting a novel route for HIV-1 transmission. *Nat Cell Biol*. 2008;10:211-219.
20. Panasiuk M, Rychlowski M, Derewonko N, Bienkowska-Szewczyk K. Tunneling nanotubes as a novel route of cell-to-cell spread of herpesviruses. *J Virol*. 2018;92:e00090-00018.
21. Dubey GP, Ben-Yehuda S. Intercellular nanotubes mediate bacterial communication. *Cell*. 2011;144:590-600.
22. Souriant S, Balboa L, Dupont M, et al. Tuberculosis exacerbates HIV-1 infection through IL-10/STAT3-dependent tunneling nanotube formation in macrophages. *Cell Rep*. 2019;26(3586-3599):e3587.
23. Gousset K, Marzo L, Commere PH, Zurzolo C. Myo10 is a key regulator of TNT formation in neuronal cells. *J Cell Sci*. 2013;126:4424-4435.
24. Omsland M, Pise-Masison C, Fujikawa D, et al. Inhibition of tunneling nanotube (TNT) formation and human T-cell leukemia virus type 1 (HTLV-1) transmission by cytarabine. *Sci Rep*. 2018;8:11118.
25. Chauveau A, Aucher A, Eissmann P, Vivier E, Davis DM. Membrane nanotubes facilitate long-distance interactions between natural killer cells and target cells. *Proc Natl Acad Sci USA*. 2010;107:5545-5550.
26. Onfelt B, Nedvetzki S, Yanagi K, Davis DM. Cutting edge: membrane nanotubes connect immune cells. *J Immunol*. 2004;173:1511-1513.
27. Andresen V, Wang X, Ghimire S, Omsland M, Gjertsen BT, Gerdes HH. Tunneling nanotube (TNT) formation is independent of p53 expression. *Cell Death Differ*. 2013;20:1124.
28. Matula Z, Nemeth A, Lorincz P, et al. The role of extracellular vesicle and tunneling nanotube-mediated intercellular cross-talk between mesenchymal stem cells and human peripheral T cells. *Stem Cells Dev*. 2016;25:1818-1832.
29. Polak R, de Rooij B, Pieters R, den Boer ML. B-cell precursor acute lymphoblastic leukemia cells use tunneling nanotubes to orchestrate their microenvironment. *Blood*. 2015;126:2404-2414.
30. Reichert D, Scheinpflug J, Karbanova J, Freund D, Bornhauser M, Corbeil D. Tunneling nanotubes mediate the transfer of stem cell marker CD133 between hematopoietic progenitor cells. *Exp Hematol*. 2016;44(1092-1112):e1092.
31. Omsland M, Bruserud O, Gjertsen BT, Andresen V. Tunneling nanotube (TNT) formation is downregulated by cytarabine and NF-kappaB inhibition in acute myeloid leukemia (AML). *Oncotarget*. 2017;8:7946-7963.
32. Hanna SJ, McCoy-Simandle K, Leung E, Genna A, Condeelis J, Cox D. Tunneling nanotubes, a novel mode of tumor cell-macrophage communication in tumor cell invasion. *J Cell Sci*. 2019;132:jcs223321.
33. Wang X, Gerdes HH. Transfer of mitochondria via tunneling nanotubes rescues apoptotic PC12 cells. *Cell Death Differ*. 2015;22:1181-1191.
34. Desir S, Wong P, Turbyville T, et al. Intercellular transfer of oncogenic KRAS via tunneling nanotubes introduces intracellular mutational heterogeneity in colon cancer cells. *Cancers (Basel)*. 2019;11:892.
35. Ahmad T, Mukherjee S, Pattnaik B, et al. Miro1 regulates intercellular mitochondrial transport & enhances mesenchymal stem cell rescue efficacy. *Embo J*. 2014;33:994-1010.

36. Rainy N, Chetrit D, Rouger V, et al. H-Ras transfers from B to T cells via tunneling nanotubes. *Cell Death Dis*. 2013;4:e726.
37. Pasquier J, Guerrouahen BS, Al Thawadi H, et al. Preferential transfer of mitochondria from endothelial to cancer cells through tunneling nanotubes modulates chemoresistance. *J Transl Med*. 2013;11:94.
38. Desir S, O'Hare P, Vogel RI, et al. Chemotherapy-induced tunneling nanotubes mediate intercellular drug efflux in pancreatic cancer. *Sci Rep*. 2018;8:9484.
39. Seyed-Razavi Y, Hickey MJ, Kuffova L, McMenamin PG, Chinnery HR. Membrane nanotubes in myeloid cells in the adult mouse cornea represent a novel mode of immune cell interaction. *Immunol Cell Biol*. 2013;91:89-95.
40. Chinnery HR, Pearlman E, McMenamin PG. Cutting edge: membrane nanotubes in vivo: a feature of MHC class II+ cells in the mouse cornea. *J Immunol*. 2008;180:5779-5783.
41. Lou E, Fujisawa S, Morozov A, et al. Tunneling nanotubes provide a unique conduit for intercellular transfer of cellular contents in human malignant pleural mesothelioma. *PLoS ONE*. 2012;7:e33093.
42. Mittal R, Karhu E, Wang JS, et al. Cell communication by tunneling nanotubes: implications in disease and therapeutic applications. *J Cell Physiol*. 2019;234:1130-1146.
43. Kolba MD, Dudka W, Zareba-Koziol M, et al. Tunneling nanotube-mediated intercellular vesicle and protein transfer in the stroma-provided imatinib resistance in chronic myeloid leukemia cells. *Cell Death Dis*. 2019;10:817.
44. Wertheim JA, Perera SA, Hammer DA, Ren R, Boettiger D, Pear WS. Localization of BCR-ABL to F-actin regulates cell adhesion but does not attenuate CML development. *Blood*. 2003;102:2220-2228.
45. Verfaillie CM, McCarthy JB, McGlave PB. Mechanisms underlying abnormal trafficking of malignant progenitors in chronic myelogenous leukemia. Decreased adhesion to stroma and fibronectin but increased adhesion to the basement membrane components laminin and collagen type IV. *J Clin Invest*. 1992;90:1232-1241.
46. Dowding C, Guo AP, Osterholz J, Siczkowski M, Goldman J, Gordon M. Interferon-alpha overrides the deficient adhesion of chronic myeloid leukemia primitive progenitor cells to bone marrow stromal cells. *Blood*. 1991;78:499-505.
47. Verfaillie CM, Bhatia R, Browne P, Key NS. Interferon-alpha restores beta1-integrin-dependent, collagen-mediated platelet aggregation in a patient with chronic myelogenous leukemia. *J Lab Clin Med*. 1998;131:163-169.
48. Bhatia R, Verfaillie CM. The effect of interferon-alpha on beta-1 integrin mediated adhesion and growth regulation in chronic myelogenous leukemia. *Leuk Lymphoma*. 1998;28:241-254.
49. Hjorth-Hansen H, Stentoft J, Richter J, et al. Safety and efficacy of the combination of pegylated interferon-alpha2b and dasatinib in newly diagnosed chronic-phase chronic myeloid leukemia patients. *Leukemia*. 2016;30:1853-1860.
50. Lee JC, Hapel AJ, Ihle JN. Constitutive production of a unique lymphokine (IL 3) by the WEHI-3 cell line. *J Immunol*. 1982;128:2393-2398.
51. Bruserud O, Gjertsen BT, Foss B, Huang TS. New strategies in the treatment of acute myelogenous leukemia (AML): in vitro culture of AML cells-the present use in experimental studies and the possible importance for future therapeutic approaches. *Stem Cells*. 2001;19:1-11.
52. McCormack E, Haaland I, Venas G, et al. Synergistic induction of p53 mediated apoptosis by valproic acid and nutlin-3 in acute myeloid leukemia. *Leukemia*. 2012;26:910-917.
53. Zunder ER, Finck R, Behbehani GK, et al. Palladium-based mass tag cell barcoding with a doublet-filtering scheme and single-cell deconvolution algorithm. *Nat Protoc*. 2015;10:316-333.
54. Hurley A, Smith M, Karpova T, et al. Enhanced effector function of CD8(+) T cells from healthy controls and HIV-infected patients occurs through thrombin activation of protease-activated receptor 1. *J Infect Dis*. 2013;207:638-650.
55. Shieh SY, Taya Y, Prives C. DNA damage-inducible phosphorylation of p53 at N-terminal sites including a novel site, Ser20, requires tetramerization. *Embo J*. 1999;18:1815-1823.
56. Silden E, Hjelle SM, Wergeland L, et al. Expression of TP53 isoforms p53beta or p53gamma enhances chemosensitivity in TP53(null) cell lines. *PLoS ONE*. 2013;8:e56276.
57. McCormack E, Mujic M, Osdal T, Bruserud O, Gjertsen BT. Multiplexed mAbs: a new strategy in preclinical time-domain imaging of acute myeloid leukemia. *Blood*. 2013;121:e34-e42.
58. Jabbour E, Kantarjian H. Chronic myeloid leukemia: 2018 update on diagnosis, therapy and monitoring. *Am J Hematol*. 2018;93:442-459.
59. Brehme M, Hantschel O, Colinge J, et al. Charting the molecular network of the drug target Bcr-Abl. *Proc Natl Acad Sci USA*. 2009;106:7414-7419.
60. Gullaksen SE, Skavland J, Gavasso S, et al. Single cell immune profiling by mass cytometry of newly diagnosed chronic phase chronic myeloid leukemia treated with nilotinib. *Haematologica*. 2017;102:1361-1367.
61. Casella JF, Flanagan MD, Lin S. Cytochalasin D inhibits actin polymerization and induces depolymerization of actin filaments formed during platelet shape change. *Nature*. 1981;293:302-305.
62. Daley GQ, Baltimore D. Transformation of an interleukin 3-dependent hematopoietic cell line by the chronic myelogenous leukemia-specific P210bcr/abl protein. *Proc Natl Acad Sci USA*. 1988;85:9312-9316.
63. Klucher KM, Lopez DV, Daley GQ. Secondary mutation maintains the transformed state in BaF3 cells with inducible BCR/ABL expression. *Blood*. 1998;91:3927-3934.
64. Obr A, Roselova P, Grebenova D, Kuzelova K. Real-time analysis of imatinib- and dasatinib-induced effects on chronic myelogenous leukemia cell interaction with fibronectin. *PLoS ONE*. 2014;9:e107367.
65. Bhatia R, Verfaillie CM. Inhibition of BCR-ABL expression with antisense oligodeoxynucleotides restores beta1 integrin-mediated adhesion and proliferation inhibition in chronic myelogenous leukemia hematopoietic progenitors. *Blood*. 1998;91:3414-3422.
66. Zaccard CR, Rinaldo CR, Mailliard RB. Linked. In: immunologic membrane nanotube networks. *J Leukoc Biol*. 2016;100:81-94.
67. Jash E, Prasad P, Kumar N, Sharma T, Goldman A, Sehrawat S. Perspective on nanochannels as cellular mediators in different disease conditions. *Cell Commun Signal*. 2018;16:76.
68. Mittal R, Karhu E, Wang JS, et al. Cell communication by tunneling nanotubes: Implications in disease and therapeutic applications. *J Cell Physiol*. 2019;234:1130-1146.
69. Van Etten RA, Jackson PK, Baltimore D, Sanders MC, Matsudaira PT, Janmey PA. The COOH terminus of the c-Abl tyrosine kinase contains distinct F- and G-actin binding domains with bundling activity. *J Cell Biol*. 1994;124:325-340.

70. Hase K, Kimura S, Takatsu H, et al. M-Sec promotes membrane nanotube formation by interacting with Ral and the exocyst complex. *Nat Cell Biol*. 2009;11:1427-1432.
71. Kretschmer A, Zhang F, Somasekharan SP, et al. Stress-induced tunneling nanotubes support treatment adaptation in prostate cancer. *Sci Rep*. 2019;9:7826.
72. Osteikoetxea-Molnar A, Szabo-Meleg E, Toth EA, et al. The growth determinants and transport properties of tunneling nanotube networks between B lymphocytes. *Cell Mol Life Sci*. 2016;73:4531-4545.
73. Apperley JF. Chronic myeloid leukaemia. *Lancet*. 2015;385: 1447-1459.
74. Dowding C, Gordon M, Guo AP, et al. Potential mechanisms of action of interferon-alpha in CML. *Leuk Lymphoma*. 1993;11(Suppl 1):185-191.
75. Minard ME, Ellis LM, Gallick GE. Tiam1 regulates cell adhesion, migration and apoptosis in colon tumor cells. *Clin Exp Metastasis*. 2006;23:301-313.
76. Forthun RB, Hellesoy M, Sulen A, et al. Modulation of phospho-proteins by interferon-alpha and valproic acid in acute myeloid leukemia. *J Cancer Res Clin Oncol*. 2019;145:1729-1749.
77. Talpaz M, Hehlmann R, Quintas-Cardama A, Mercer J, Cortes J. Re-emergence of interferon-alpha in the treatment of chronic myeloid leukemia. *Leukemia*. 2013;27:803-812.
78. Mitchell R, Hopcroft LEM, Baquero P, et al. Targeting BCR-ABL-independent TKI resistance in chronic myeloid leukemia by mTOR and autophagy inhibition. *J Natl Cancer Inst*. 2018;110:467-478.
79. Eiring AM, Page BDG, Kraft IL, et al. Combined STAT3 and BCR-ABL1 inhibition induces synthetic lethality in therapy-resistant chronic myeloid leukemia. *Leukemia*. 2015;29:586-597.
80. Hehlmann R. How I treat CML blast crisis. *Blood*. 2012;120: 737-747.
81. Barnes DJ, Palaiologou D, Panousopoulou E, et al. Bcr-Abl expression levels determine the rate of development of resistance to imatinib mesylate in chronic myeloid leukemia. *Cancer Res*. 2005;65:8912-8919.
82. Pietarinen PO, Eide CA, Ayuda-Duran P, et al. Differentiation status of primary chronic myeloid leukemia cells affects sensitivity to BCR-ABL1 inhibitors. *Oncotarget*. 2017;8:22606-22615.
83. Pemovska T, Johnson E, Kontro M, et al. Axitinib effectively inhibits BCR-ABL1(T315I) with a distinct binding conformation. *Nature*. 2015;519 :102-105.
84. Houshmand M, Simonetti G, Circosta P, et al. Chronic myeloid leukemia stem cells. *Leukemia*. 2019;33:1543-1556.
85. Caponetti GC, Bagg A. Genetic studies in the evaluation of myeloproliferative neoplasms. *Semin Hematol*. 2019;56:7-14.
86. Valent P, Sadovnik I, Eisenwort G, et al. Redistribution, homing and organ-invasion of neoplastic stem cells in myeloid neoplasms. *Semin Cancer Biol*. 2019. pii: S1044-579X(19)30214-7.
87. Griessinger E, Moschoi R, Biondani G, Peyron JF. Mitochondrial transfer in the leukemia microenvironment. *Trends Cancer*. 2017;3:828-839.
88. Burt R, Dey A, Aref S, et al. Activated stromal cells transfer mitochondria to rescue acute lymphoblastic leukaemia cells from oxidative stress. *Blood*. 2019;34:1415-1429.
89. Bewry NN, Nair RR, Emmons MF, Boulware D, Pinilla-Ibarz J, Hazlehurst LA. Stat3 contributes to resistance toward BCR-ABL inhibitors in a bone marrow microenvironment model of drug resistance. *Mol Cancer Ther*. 2008;7:3169-3175.
90. Weisberg E, Wright RD, McMillin DW, et al. Stromal-mediated protection of tyrosine kinase inhibitor-treated BCR-ABL-expressing leukemia cells. *Mol Cancer Ther*. 2008;7:1121–1129.
91. Kumar A, Bhattacharyya J, Jaganathan BG. Adhesion to stromal cells mediates imatinib resistance in chronic myeloid leukemia through ERK and BMP signaling pathways. *Sci Rep*. 2017;7:9535.
92. Lundell BI, McCarthy JB, Kovach NL, Verfaillie CM. Activation-dependent alpha5beta1 integrin-mediated adhesion to fibronectin decreases proliferation of chronic myelogenous leukemia progenitors and K562 cells. *Blood*. 1996;87:2450-2458.
93. Zhang B, Li M, McDonald T, et al. Microenvironmental protection of CML stem and progenitor cells from tyrosine kinase inhibitors through N-cadherin and Wnt-beta-catenin signaling. *Blood*. 2013;121:1824-1838.
94. Krause DS, Scadden DT. A hostel for the hostile: the bone marrow niche in hematologic neoplasms. *Haematologica*. 2015;100:1376-1387.
95. Duarte D, Hawkins ED, Lo Celso C. The interplay of leukemia cells and the bone marrow microenvironment. *Blood*. 2018;131:1507-1511.
96. Podszywalow-Bartnicka P, Cmoch A, Wolczyk M, et al. Increased phosphorylation of eIF2 alpha in chronic myeloid leukemia cells stimulates secretion of matrix modifying enzymes. *Oncotarget*. 2016;7:79692-79707.
97. Reikvam H, Skavland J, Gullaksen SE, et al. Chronic myeloid leukemia relapsing 25 years after allogenic stem cell transplantation. *Case Rep Hematol*. 2018;2018:2045985.

SUPPORTING INFORMATION

Additional supporting information may be found online in the Supporting Information section.

How to cite this article: Omsland M, Andresen V, Gullaksen S-E, et al. Tyrosine kinase inhibitors and interferon-α increase tunneling nanotube (TNT) formation and cell adhesion in chronic myeloid leukemia (CML) cell lines. *The FASEB Journal*. 2020;34:3773–3791. https://doi.org/10.1096/fj.201802061RR